Journal of Materials Chemistry

Cite this: *J. Mater. Chem.*, 2012, **22**, 4216

www.rsc.org/materials

FEATURE ARTICLE

Prospects and challenges of organic/group IV nanomaterial solar cells

Tao Song,[a] Shuit-Tong Lee[b] and Baoquan Sun*[a]

Received 2nd October 2011, Accepted 26th January 2012
DOI: 10.1039/c2jm14943e

Organic/group IV nanomaterial-based solar cells attract wide research interest in the photovoltaic community because it can benefit from the advantages of both organic and group IV materials. Especially, hybrid composites of conjugated organic materials and nanostructured inorganic materials are potential candidates for cost-effective and efficient solar-energy-harvesting devices. This review highlights recent advances in organic photovoltaics (OPV) as well as organic-inorganic hybrid solar cells (HSCs) based on group IV nanomaterials, including nanostructured carbon and silicon materials which act as acceptors. The donor can be either small molecules or conjugated polymers. The carbon-based functional materials will vary from carbon nanotubes (CNTs) to new emerging graphene sheets, which do not include fullerene and its derivatives. The silicon nanostructures include free-standing silicon nanocrystals (NCs) and silicon nanowires (SiNWs).

1. Introduction

Conjugated organic materials exhibit several merits for photovoltaic (PV) applications, such as large light absorption coefficient for efficient light harvesting, strong π–π stacking interactions for charge transfer, low-cost solution processability, and soft mechanical behaviour for future flexible devices.[1] In traditional inorganic crystalline solar cells, p–n homojunctions and heterojunctions are the fundamental components for PV response. The built-in potential across the junction is the driving force to separate photo-induced electron-hole pairs and sweep

[a]*Jiangsu Key Laboratory for Carbon-Based Functional Materials & Devices, Institute of Functional Nano & Soft Materials (FUNSOM), Soochow University, 199 Ren'ai Road, Suzhou, 215123, China. E-mail: bqsun@suda.edu.cn; Fax: +0086-512-65882846; Tel: +0086-512-65880951*

[b]*Center of Super-Diamond and Advanced Films (COSDAF) and Department of Physics and Materials Science, City University of Hong Kong, Hong Kong SAR*

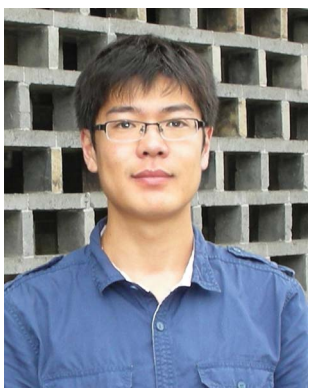

Tao Song

Tao Song received his Masters of Science degree in Physics at Soochow University in 2009. The subjects of his thesis were quantum information and computation. Since 2009, he has been pursuing his PhD work in Institute of Functional Nano & Soft Materials (FUNSOM), Soochow University. His main research interest is focused on hybrid solar cells based on colloidal semiconductor nanocrystals and conjugated polymers, as well as silicon nanowire array-based photovoltaics.

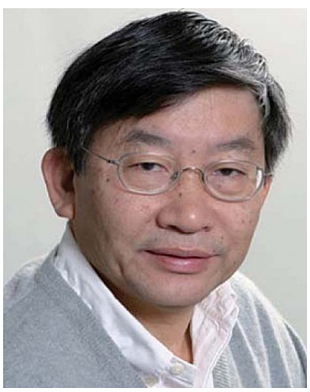

Shuit-Tong Lee

Shuit-Tong Lee is a member (academician) of the Chinese Academy of Sciences (CAS) and fellow of the academy of sciences for the developing world (TWAS). He is a Chair Professor of Materials Science and Director of the Center of Super-Diamond and Advanced Films (COSDAF) at City University of Hong Kong, Director of Institute of Functional Nano & Soft Materials (FUNSOM) at Soochow University, and Director of Nano-Organic Photoelectronic Laboratory at the Technical Institute of Physics and Chemistry, CAS. His major research areas include functional nanomaterials and devices, organic electronic materials and technologies, diamond and super-hard thin film technologies.

them to the corresponding electrodes. In organic semiconductors, strongly bound excitons, which are actually electron-hole pairs in single or triplet spin states, are generated upon absorbing photons. Excitons can diffuse in organic materials with a typical diffusion length of ~10–20 nm before recombination occurs. If excitons could reach the interface between the donor and acceptor within their lifetime, the strong built-in field would dissociate them into separate electron and hole pairs, which is commonly accepted as the origin of organic PV effects. In 1986, the construction of the very first organic solar cell was reported by Tang,[2] exhibiting a preliminary power conversion efficiency (PCE) of 0.95%. The device had a bilayer structure with copper phthalocyanine (CuPc) as donor and a perylene tetracarboxylic derivative as acceptor sandwiched between transparent indium tin oxide (ITO) coated glass and metal electrodes. This pioneering achievement demonstrated the feasibility of employing semiconducting organic materials to convert solar energy into electrical power.

Since the photoactive layers were composed of only organic materials, this kind of solar cell was defined as organic photovoltaics (OPV), and Tang's work was considered as the cornerstone of OPV. Since the diffusion length is very short in organic materials, only the excitons generated near the donor–acceptor interfaces can be dissociated. In order to obtain a high PCE, larger interface area is required for efficient exciton dissociation. Meanwhile, both the donor and acceptor materials have to form percolative networks in the active layer for transporting the separated charge carriers to their corresponding electrodes. To achieve this, the concept of bulk heterojunction (BHJ) structure was proposed and experimentally demonstrated by a range of methods, such as co-evaporation of small molecules[3] and solution casting of mixed conjugated polymers[4] or blends of small molecules/conjugated polymer.[5] However, the modest PV performance of these all-organic BHJ solar cells (BHSCs) based on polymer and small molecules is much lower than traditional inorganic solar cells. The poor electron mobility of n-type organic semiconductors compared with p-type counterparts is one of the main drawbacks in these OPV applications. As a result of the unbalanced electron and hole transport in active layers, the photogenerated electrons tend to accumulate at the donor–acceptor interfaces forming a space charge region that leads to inefficient charge transport and extensive recombination.[6] In order to enhance the mobility of acceptor materials and realize a matched electron and hole mobility, it is intriguing to develop new organic acceptors with high electron mobility.[7,8] So far, fullerene and its derivatives are very successful organic acceptors widely used in OPV. The highest PCE of BHSCs based on [6,6]-phenyl C_{71} butyric acid methyl ester ($PC_{71}BM$) and conjugated polymer PTB7 has already reached 8.37%.[9] In June 2011, Mitsubishi Chemical reported the world's highest PCE of 10.1% in small molecule-based OPV on their website (www.m-kagaku.co.jp). This state-of-the-art PCE has exceeded the commonly reckoned benchmark (~10%) for commercialization of OPV. They are now expecting a volume production of OPV modules in 2015. In this review, we would like to steer clear of photovoltaics based on fullerene and its derivatives, since there are already several detailed reviews about fullerene/organic semiconductor BHSCs.[1,10]

The mobility of typical crystalline inorganic semiconductors is in the range of $\sim 10^4$ $cm^2V^{-1}s^{-1}$, which is several orders higher than that in organic materials ($\sim 10^{-3}$–10 $cm^2V^{-1}s^{-1}$). Besides, compared with organic semiconducting materials, inorganic semiconductors exhibit inherently better stability against oxygen and moisture, which is very important for the reliability of solar cells in ambient atmosphere. Solar cells employing organic and inorganic hybrid materials as the photoactive layer have the potency to benefit from the advantages of both organic and inorganic components. By rationally designing the electrical and optical characteristics of the hybrid system, the construction of high-performance low-cost solar cells is potentially possible. Because both organic and inorganic phases exist in the photoactive region and contribute to the PV effect, these solar cells were defined as hybrid solar cells (HSCs).

Nanotechnology is now undergoing rapid developments in many applications with fruitful achievements. Nanoscale science and engineering have become interdisciplinary subjects involving many traditional scientific fields such as bio-medical applications, electronics, power storage and conversion of solar energy. Compared to the bulk form, nanomaterials exhibit unique properties when the characteristic length comes to nano or submicron scale, for example, extremely large surface area to volume ratio for sensing and catalysis, tunable luminescence for *in vivo* diagnosing or light emitting, and solution processability for large-scale low-cost PV applications. One of the fundamental interests of nanotechnology investigation is to utilize the advanced nanoscale science and engineering techniques to improve the performances of commercially available products and lower the production cost. The fast developing nanoscale fabrication and processing technologies allow direct observation and examination of nano-structured materials. A range of functional devices have been fabricated on individual nanostructures *via* nanotechnology such as electron beam lithography. And the corresponding devices display promising performance. Though the results are exciting, the dedicated fabrication processes are expensive and time-consuming which is apparently not compatible with volume production. By solution processing techniques, thin films or bulk composites based on nanomaterials could be facilely prepared. As-made films and

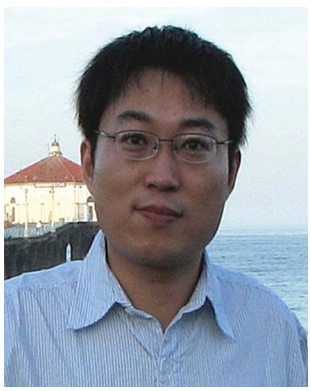

Baoquan Sun

Baoquan Sun received his PhD in Chemistry at Tsinghua University in Beijing in 2002. After being a postdoc. in Prof. Friend's group in Cavendish Laboratory at Cambridge University and in Dr Klimov's group at Los Alamos National Laboratory, he joined Institute of Functional and Soft Materials (FUNSOM) at Soochow University in Suzhou, China in 2008. His main research field is dedicated to the physical characterization of conjugated polymer and semiconductor nanostructures, their application in hybrid solar cells and thin film field-effect transistors.

composites are of macroscopic scale, so traditional fabrication technologies are readily applicable.

Nanotechnology brings several new concepts and possibilities into PV applications. Many inorganic nanomaterials are introduced into the matrix of organic semiconductors to fabricate BHJ HSCs. Semiconductor nanocrystals (NCs) have attracted extensive attention due to their promising performances in solar cells, such as ZnO,[11] CdS,[12,13] CdSe,[13–15] PbS[16,17] and PbSe[18] NCs of groups II–VI, InAs[19,20] quantum dots (QDs) of groups III–V, and C,[21,22] Si,[23] Ge[24] QDs of group IV semiconductors.

An ordered nanostructure has better light trapping ability compared with a planar wafer, because the incident light can be scattered several times before escaping the textured substrates. Especially, three dimensional arrays of vertically aligned nano- or micro-wires present superior antireflection properties; meanwhile, these quasi-one-dimensional wires with high aspect ratio provide unique radial pathways for efficient charge carrier transfer. The enhanced PV performances have been experimentally demonstrated in solar cells based on three-dimensional nanowire arrays of group II–VI semiconductor ZnO,[25] group III–V semiconductor GaAs,[26] and group IV semiconductor Si.[27–29]

The optoelectrical properties of carbon based nanomaterials, especially the new emerging graphene, have attracted enormous interest. Silicon, as the traditional "old" PV material, still plays the dominant role in the commercial solar cell market. In addition, organic semiconductors, due to their specific properties, are regarded as alternative photoactive materials for future plastic electronic applications. This review highlights recent developments and challenges in OPV and HSCs based on carbon and silicon nanostructured materials of group IV. Organic materials can be either small molecules like copper phthalocyanine (CuPc) and porphyrin, or conjugated polymers like poly(3-hexylthiophene) (P3HT) and poly[2-methoxy-5-(2-ethylhexyloxy)-1,4-phenylenevinylene (MEH-PPV). The carbon based nanomaterials include carbon nanotubes (CNTs) and graphene sheets, which are classified separately from fullerene and its derivatives. The silicon nanostructures consist of free-standing silicon NCs and silicon nanowires (SiNWs). The schematics of BHJ and aligned wire array structures, as well as the typical conjugated organic materials and group IV nanostructures involved in this review are depicted in Fig. 1.

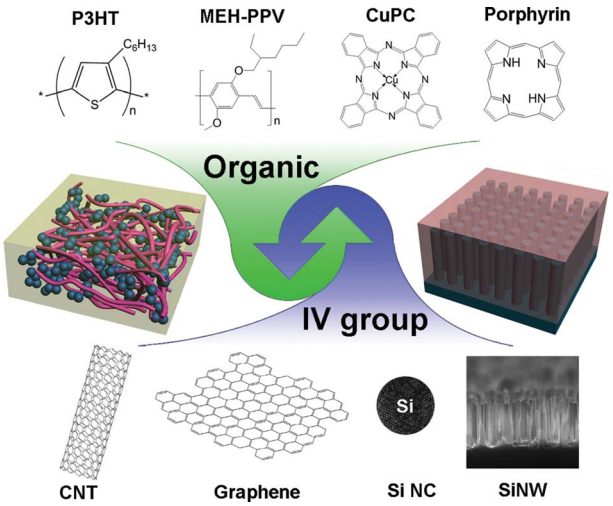

Fig. 1 Schematics of BHJ structure and ordered nanowire array structure. The typical conjugated organic materials and group IV nanostructures are also illustrated.

2. Carbon-based OPV

CNT is one of the most studied nanomaterials so far. It is a representative model of typical sophisticated nanomaterials, demonstrating many common microscopic properties, such as bandgap tuning, functionalization, and solution processability. Meanwhile, CNTs also have some unique merits for fabrication of novel nanodevices, for example, high conductivity and transparency for electrode applications in touch panels or PV devices; extremely large surface to volume ratio for sensors, supercapacitors, catalysis and energy storage; high mechanical strength for robust flexible composites. Especially, the mobility of high quality CNTs is in the order of $\sim 10^4$ $cm^2V^{-1}s^{-1}$, which is much larger than other nanomaterials and organic semiconductors (typically $\sim 10^{-3}$ to 10 $cm^2V^{-1}s^{-1}$). In addition, the electrical properties of CNTs can be carefully controlled by modifying the synthetic conditions and subsequent chemical modifications.[30] Due to these superior properties, CNTs are considered as the essential nanomaterials to obtain sustainable energy from solar power in the future. There are two kinds of CNTs according to their physical structures: single-walled carbon nanotube (SWNT) formed by wrapping a single layer of sp^2 hybridized carbon atoms into a roll; and multiple-walled carbon nanotubes (MWNT) composed of several SWNTs with different diameters arranged in a concentric structure. The MWNTs exhibit conductive behaviour with good chemical stability. MWNT films are extensively investigated as flexible transparent electrodes for PV devices,[31] since the commonly used ITO glasses are expensive and contain the rare metal indium. The situation is different with SWNTs. Both semiconducting SWNTs (s-SWNTs) and metallic SWNTs (m-SWNTs) exist in the as-synthesized products. These two species can be distinguished by the (n, m) indices of the circumference vector. The SWNTs with type +1 or type −1 for $n - m = 3i + 1$ and $n - m = 3i - 1$ present semiconducting behaviours, while the others are metallic.[32,33] SWNTs present the intrinsic nature of CNTs because there are fewer defects on SWNT sidewalls compared with those on MWNTs. However, the cost of SWNTs is ~50 times higher than that of MWNTs as well. CNTs can act as acceptor materials in BHSCs with their semiconductor characteristics or play the role of charge transfer pathways with their conductive characteristics. Here, CNTs as electrodes will not be discussed due to the length limitation of the paper, meanwhile, there are already several comprehensive reviews in this field.[34,35]

Graphene is a two dimensional single layer of carbon atoms with sp^2 hybridization, which was first obtained experimentally by mechanical exfoliation method in 2004.[36] Mobility as high as $\sim 10^4$ $cm^2V^{-1}s^{-1}$ was measured in graphene sheets at room temperature, which is comparable with that in high quality CNTs and several orders higher than the typical mobility in organic semiconductors. The excellent electrical properties and flexible nature make it a superior optoelectronic carbon nanomaterial alongside fullerene and CNTs.[37] But the preparation of high

quality graphene single layers is time consuming and less productive, which is apparently impractical for large scale application. Solution processed techniques provide the possibility to massively manufacture graphene sheets with moderate quality by first oxidizing graphite into graphene oxide (GO) sheets and subsequently reducing the GO sheets by physical or chemical methods to partially restore the electrical properties of graphene. We will focus exclusively on the solution processed graphene materials hereafter. There are enormous functional groups on GO sheets readily available for various chemical modifications, rendering the solution processed graphene sheets as an ideal arena for investigation of organic composites.[38–41] A range of functional composites and devices employing graphene and organic semiconducting materials have been constructed showing promising performances in many fields, such as acceptor materials in BHSCs,[42–44] flexible transparent electrodes for OPV and organic light emitting (OLED) devices,[45–47] free-standing electrodes for batteries and supercapacitors,[48] nonvolatile memory devices,[49] nonlinear optical and optical limiting composites.[50,51] Since the theme of this review is to unfold the specific PV properties of OPV and HSCs, the applications of graphene sheets as transparent electrode in solar cells are not included here.

2.1 OPV based on carbon nanomaterials/conjugated polymer

The first OPV employing a blend film of SWNTs and conjugated polymer poly(3-octylthiophene) (P3OT) as the active layer was reported in 2002.[52] It opened up a new approach to manufacture OPV devices by incorporating CNTs as acceptor materials instead of commonly used fullerene molecules. The CNTs also provided percolation pathways to transport photo-induced electrons to the cathode. Two orders higher short-circuit current (J_{sc}) and doubled open-circuit voltage (V_{oc}) were obtained compared with pristine diodes made of P3OT without CNTs. In these BHSCs, the V_{oc} was larger than the theoretical limit predicted by the metal-insulator-metal (MIS) model. By studying the current–voltage (I–V) characteristics, it was suggested that the internal junctions formed between polymer and CNTs enhanced the photoinduced charge separation and transportation in the blend, finally leading to the larger experimental V_{oc} than the theoretical maximum in the MIS model. The V_{oc} was suggested to be proportional to the difference between the highest occupied molecular orbital (HUMO) of the conjugated polymer and the work function of SWNTs.[53]

The photogenerated excitons in conjugated polymer could be dissociated into separated electron-hole pairs at the interface of SWNTs/conjugated polymer. Photoluminescence excitation (PLE) spectroscopy measurements on specific SWNTs revealed that type II heterojunctions were formed between P3HT and s-SWNTs with small diameters.[33,54] Theoretical study of the interfaces between P3HT and SWNTs showed that P3HT polymer backbones could self-assemble around CNTs in diverse conformations like helices, bundles, and more elongated conformations that maximized planar π–π stacking, revealing that the CNTs could template and enhance the π–π conjugation in the blend. The increased conjugation contributed to the charge dissociation processes in type II P3HT/s-SWNTs heterojunctions.[55] Thiophene groups grafted at the edges and defects of SWNTs were found to improve the compatibility between conjugated polymer and SWNTs. The covalently anchored thiophene groups on SWNTs led to enhanced exciton dissociation.[56] Pyrene functionalized P3HT derivative could be non-covalently attached to SWNTs by π–π bonding interactions. The significant fluorescence intensity quenching of polymer derivatives indicated efficient exciton dissociation processes between SWNTs and P3HT bridged by pyrene moieties.[57] The choice of organic solvents to dissolve both conjugated polymer and SWNTs affects the dispersion of the blended materials and the amount of effective organic-inorganic interfaces which is in proportion to the exciton dissociation probability. Chloroform and chlorobenzene were found to be good solvents in dispersing the mixture of P3HT and SWNTs. Better PV performance was achieved in comparison to devices cast from other solvents.[58] In order to investigate the properties of the intrinsic interfaces between semiconducting polymers and SWNTs, planar nano-heterojunction devices comprising P3HT and laterally aligned ultra-long SWNT arrays on Si substrates with insulating SiO_2 layers were constructed as depicted in Fig. 2. A polyethylene imine (PEI) coating was applied to convert the SWNTs from p-type to n-type for a preferred band alignment. The average PCE of individual SWNT was 3%, which proved the efficient exciton dissociation processes at the conjugated polymer/SWNTs interfaces.[59] Therefore, the primary reason for the inferior PCE in conjugated polymer/SWNTs BHSCs is probably due to the formation of bundled SWNT aggregates and extensive tube-tube type recombination processes between s-SWNTs and m-SWNTs.

The transport ability in typical organic materials is usually inferior to that in CNTs. Since the SWNTs have excellent charge transporting properties, adding SWNTs into conjugated polymer is expected to improve the charge carrier transport in blend films. Incorporation of SWNTs in an organic donor matrix led to

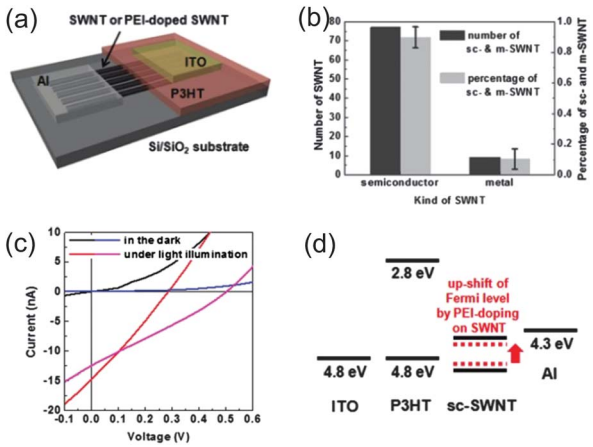

Fig. 2 PV device based on n-type SWNTs displayed a large PCE. (a) Schematic of the nano-heterojunction PV device based on a P3HT film coated on laterally aligned SWNTs. (b) The number and percentage of s-SWNTs and m-SWNTs in CVD-grown CNTs. (c) I–V curves of the nano-heterojunction devices with p-type SWNTs (black and red) and n-type SWNTs (blue and pink) in the dark and under simulated AM 1.5 illumination at 100 mWcm^{-2}. (d) The energy diagram of the P3HT/SWNT heterojunction. (Reprinted from ref. 59 with permission. Copyright 2010 American Chemical Society.)

a higher PCE than that of a reference device without SWNTs, because of enhanced photogenerated charge transport in the active layers.[60]

In addition, the strong interaction between SWNTs and conjugated polymers was favourable to enhance the crystallinity of the active layer. Sub-micrometre sized crystal domains of P3HT were observed on the sidewalls of SWNTs.[61] PV devices could benefit from the enhanced conjugation in better crystallized organic semiconductors. And a higher V_{oc} value was obtained due to the HOMO level reduction of SWNTs.

Since there exist both s-SWNTs and m-SWNTs in as-synthesized products without further separation processes, the detailed contribution of these two components to PV performance is thus an interesting subject to investigate. The simulation based on a density function theory approach demonstrated that a type II heterojunction could be formed at the interfaces between s-SWNTs and P3HT which is desirable for PV devices. However, m-SWNTs interact strongly with conjugated polymers leading to an unfavourable ultra-small built-in potential. These results indicated that the performance of SWNTs/conjugated polymer OPVs was generally limited by the inefficient interfaces with m-SWNTs.[62] In another study, the PV device based on a single P3HT/SWNT nano-heterojunction demonstrated efficient photocurrent generation irrespective of whether s-SWNTs or m-SWNTs were used,[63] which is shown in Fig. 3. The built-in potential caused by the work function difference between SWNTs and P3HT led to efficient exciton dissociation and hole transfer. External quantum efficiency (EQE, also called incident photon to photocurrent efficiency, IPCE) more than 90% was obtained in millimetre scale P3HT/SWNTs solar cells fabricated on a lateral array of SWNTs. The P3HT/SWNTs heterojunction devices exhibited promise for high-performance low-cost flexible OPV applications.

MWNTs are also important building blocks for BHJ OPV. An aqueous blend solution of acid-oxidized MWNTs and the water-soluble conjugated polymer sodium poly[2-(3-thienyl)-ethoxy-4-butylsulfonate] (PTEBS) was used to cast the active layers on ITO substrates. Fullerene was vacuum deposited on the blend films to fabricate PV devices. A moderate PCE of 0.56% was obtained.[64] SWNTs and MWNTs with diverse diameters and lengths were incorporated in organic solar cells to study the effects of CNT variation. It was found that short SWNTs with 2–8 nm diameter and long MWNTs with 10–20 nm diameter were preferred to get a high PCE, and a CNT concentration of 5% was optimal for PV performances.[65] SWNTs were expected to improve exciton dissociation and electron transport, while MWNTs contributed to hole transfer.[66]

Several mechanisms were proposed to explain the beneficial effects of MWNTs mixed in conjugated polymers. In the MWNTs/PPV blend, clear evidence of non-radiative energy transfer (NRET) of excitons from conjugated polymer to MWNTs has been identified through photoluminescence (PL) and photoinduced absorption (PIA) spectroscopy. The slightly reduced π–π conjugation indicated a certain degree of disorder in conjugated polymer induced by MWNTs.[67] Core-shell structured P3HT/MWNT heterojunction nanotubes were fabricated by electrochemical deposition techniques,[68] as shown in Fig. 4. By studying the *I–V* response of a single heterojunction nanotube, it was found that the outer P3HT shell showed semiconducting behaviour, while Ohmic behaviour was observed for the inner MWNT core. And the heterojunction formed at the P3HT/MWNT interface presented rectification behaviour which could be properly described by the Fowler–Nordheim tunnelling model.[68]

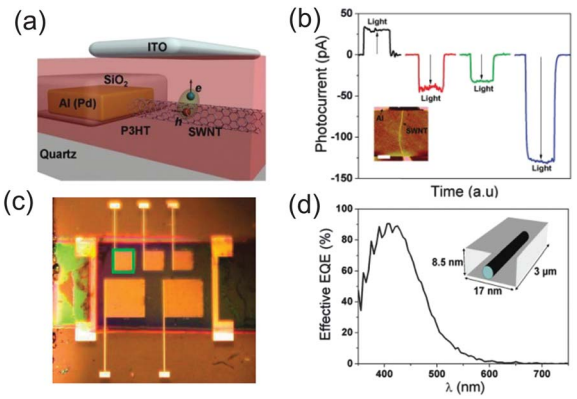

Fig. 3 Both s-SWNTs and m-SWNTs accept holes from P3HT as revealed by PV devices based on an individual P3HT/SWNT heterojunction. (a) Schematic of the single heterojunction device. (b) J_{sc} for an individual P3HT/s-SWNT junction (red line), an individual m-SWNT/P3HT junction (green line), an ensemble P3HT/SWNT device containing six nanotubes (blue line), and an Al/P3HT reference device (black line). The devices were illuminated by a continuous wave 532 nm laser at 1275 mWcm^{-2}. The inset shows the atomic force microscope (AFM) image of a single SWNT between electrical contacts. Scale bar is 2 μm. (c) Optical image of large area devices. Scale bar is 1 mm (green box). (d) Estimated effective EQE of a single junction heterojunction. Effective volume of a single heterojunction was considered as a rectangular box. (Reprinted from ref. 63 with permission. Copyright 2011 American Chemical Society.)

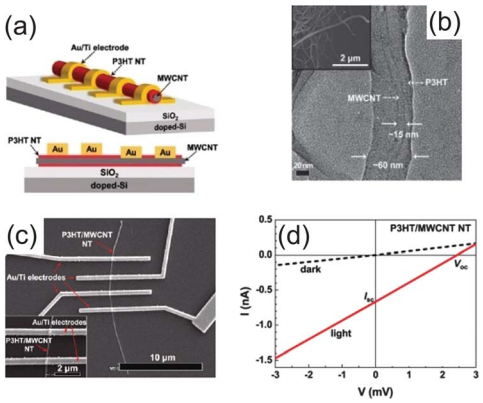

Fig. 4 PV device based on an individual MWNT-P3HT core-shell nanotube. (a) Schematic and cross sectional view of device structure using a single heterojunction nanotube with four-probe Au/Ti electrodes. (b) High resolution transmission electron microscopy (HRTEM) image of a MWNT wrapped by P3HT. Inset shows the scanning electron microscope (SEM) image of a core-shell structured nanotube. (c) SEM image of as-made PV device. Inset shows magnified contact of single nanotube with Au/Ti. (d) *I–V* curves of an individual P3HT/MWNT nanotube PV device in the dark and under 100 mWcm^{-2} illumination. (Reprinted from ref. 68 with permission. Copyright 2010 American Chemical Society.)

Furthermore, the mobility enhancement in MWNT blended conjugated polymer films was also observed in thin film transistor (TFT) devices.[69] MWNTs mixed in P3HT not only act as conducting bridges among crystallize domains of conjugated polymer, but also reduce the hole injection barrier since they have lower work function. P3HT chains were covalently attached onto MWNTs to enhance the dispersion of MWNTs in organic solvent.[70] Determined by TFT characteristics, the blend film composed of P3HT grafted MWNTs and pure P3HT showed increased field-effect mobility compared with P3HT only films or simple P3HT/MWNTs blend films without covalent bonding. The hole mobility in the conjugated polymer was influenced by the morphology of the polymer backbone packing. The presence of CNTs led to positional disorder in conjugated polymer films, which converted the non-dispersive transport with positive field dependent mobility in pure polymer films into dispersive transport and negative field dependent mobility in polymer/CNTs blend films, as detected by time of flight (TOF) measurements.[71]

The boosted PV performances by incorporating CNTs in BHSCs can be explained by percolation theory as well. The conductivity of a conjugated polymer will be enhanced by several orders of magnitude because a percolation CNT network can be formed if the CNT fraction exceeds the percolation threshold.[72] A threshold value of ~0.7% to 1% was estimated in P3HT/SWNTs blend films, inferred from capacitance–voltage and *I–V* measurements.[73] At lower SWNTs concentration, the bipolar charge injection is enhanced. By further increasing the SWNT fraction in blend films, the exciton dissociation becomes the dominant process, leading to better photoresponse.[74] The calculated effective mobility first increases with CNT concentration to a maximum value, then decreases with higher CNT fraction, which is coincident with the PV performance dependence on CNT addition.[72,75] By studying the temperature-dependent conductivity of P3HT/MWNTs blend films with different MWNT concentration, it was concluded that the conduction mechanism shifted from variable-range hopping to fluctuation-assisted tunnelling with higher MWNT fraction.[76]

Functionalization could modify the optoelectrical behaviour of CNTs, which may be beneficial to OPV devices. Dye functionalized SWNTs facilitate the exciton dissociation and charge carrier transportation in the blend of polymer/dye-attached SWNTs.[77] The C_{60}-SWNT composites synthesized by a microwave irradiation approach were blended with P3HT to construct BHSCs. Compared with the control device without SWNTs, enhanced PV effect was obtained using C_{60}-SWNTs as acceptor materials.[78] Fullerene peapods prepared by encapsulating C_{60} or C_{70} molecules in SWNTs were capable of completely quenching the fluorescence of P3HT. However, no remarkable difference in photodynamics was observed in comparison with pristine SWNTs in steady and time-resolved spectroscopic measurements.[79] Covalent attachment of semiconductor QDs onto SWNTs has the potential to tune the optoelectronic properties by facilitating exciton dissociation and charge transport in BHSCs.[80] Indeed, a higher J_{sc} has been obtained experimentally in PV devices based on blend films of P3OT/CdSe QD-attached SWNTs.[81] Thiol groups anchored onto SWNTs by reaction with cysteamine were also reported to enhance PV performance of BHSCs.[82] The attached thiol groups are readily applicable for further functionalization of semiconductor or metal NCs. PbSe QDs were anchored onto the sidewalls of SWNTs by functionalized thiol groups to expand the absorption range of BHSCs to the infrared region. The PV devices based on blend films of poly(vinyl carbazole)/PbSe QD-grafted SWNTs exhibited an IPCE of 2.6% upon infrared light illumination, which was two times larger than the control device without SWNTs.[83]

Fullerene based molecules are an essential group of carbon nanomaterials with interesting optoelectronic properties and have been investigated extensively in OPV applications.[84,85] A solar cell based on blend films cast from a mixture of MWNTs and P3HT/[6,6]-phenyl C_{61} butyric acid methyl ester (PCBM) (1 : 1, w/w) blend showed a PCE of 2% for an optimal MWNT concentration of 0.1%. The PCE was nearly 3 times larger than that of the device without MWNT addition,[86] which is shown in Fig. 5. From the AFM image of the P3HT:PCBM:MWNTs blend film, it could be observed that the film morphology was homogeneous with uniformly distributed P3HT crystallized domains, indicating the enhanced structuring of the conjugated polymer in the presence of MWNT dispersion. Similar PV devices using SWNTs functionalized with carboxyl groups prepared by acid treatment instead of high-purity pristine SWNTs, exhibited a poorer PCE of 1.4%, which was probably due to the high-density defects in functionalized SWNTs.[87] The presence of defects in SWNTs was found to disrupt the electron transfer from P3HT to SWNTs, indicating the quality of CNTs played an essential role in OPV devices.[88] Thiophene, amine groups and both of them were grafted onto MWNTs to improve the dispersion in a photoactive composite solution, and improved PCE was obtained by using thiophene and thiophene-amine functionalized MWNTs.[89] In conjugated polymer/fullerene derivative BHSCs, the addition of CNTs could improve the PV performance for several reasons. As inferred from the results of intensity dependent photocurrent measurement, the presence of m-SWNTs is responsible for bimolecular recombination in the active layer, and the s-SWNTs provide low-resistance pathways for improved charge transport.[90] MWNT doping effects in P3HT/PCBM BHSCs were also studied. PCE as high as 3.47% was obtained by adding only 0.01% fraction of MWNTs into the active layers,[91] as shown in Fig. 6. By applying Kelvin probe force microscopy (KPFM) techniques, it was revealed that the positive shift of work function in P3HT rich domain under light illumination was corresponding to the doping effect of MWNTs. The PV performance improvements were attributed to increased light absorption of better aligned polymer chains and balanced work function alignment due to MWNT addition.

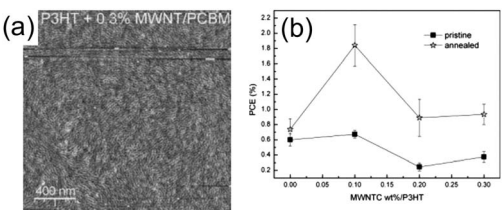

Fig. 5 Solar cell based on a blend of MWNTs:P3HT:PCBM. (a) AFM image of P3HT:PCBM (1 : 1, w:w) + 0.3 wt% MWNT blend film. (b) The evolution of PCE *versus* the concentration of MWNTs in P3HT:PCBM active layer. (Reprinted with permission from ref. 86. Copyright 2007 John Wiley and Sons.)

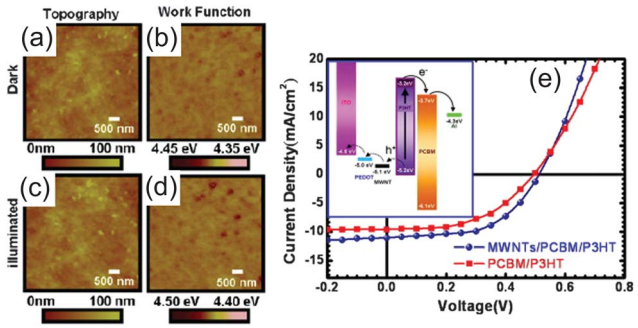

Fig. 6 MWNTs (0.10% by weight) led to enhanced PV performance of BHSCs with ITO/PEDOT:PSS/P3HT:PCBM:MWNTs/Al structure. (a,b) Morphology image and work function mapping image of the active layer in the dark. (c,d) Morphology image and work function mapping image of the active layer under illumination. (e) *I–V* characteristics of BHSCs with and without MWNTs measured under AM 1.5 100 mWcm^{-2} illumination. Inset image presents the energy levels in the solar cells. (Reprinted from ref. 91, Copyright 2009, with permission from Elsevier.)

Transfer of photogenerated holes from P3HT to SWNTs was also observed in KPFM measurements, suggesting that the SWNTs acted as donor materials in the SWNTs/conjugated polymer blend.[92] The amount of SWNTs in the P3HT/PCBM BHSCs is closely correlated with the PV performance. With optimal SWNT concentration, both the effective mobility and electrode contact area were increased, resulting in reduced series resistance and higher fill factor (FF) for efficient charge collection through SWNTs to electrodes. As shown in Fig. 7, a PCE of 3.52% was obtained with 0.75% SWNT fraction in P3HT:PCBM (1 : 1, wt/wt) blend films under weak light illumination, which was 23% larger than that of the reference cell without SWNTs.[93] In comparison with pristine P3HT, the lowest unoccupied molecular orbital (LUMO) and the HOMO energy levels are lower in P3HT covalently grafted on acid-oxidized MWNTs. The energy level shift leads to an increment of energy difference between the LUMO of fullerene acceptor and the HOMO of conjugated polymer donor in active layers, which accounts for the increased V_{oc} in PV characteristic measurements.[94] Furthermore, bandgap narrowing phenomenon in P3HT covalently grafted onto MWNTs was detected.[95] The decreased bandgap of the conjugated polymer extended the absorption range leading to more efficient light harvesting in BHSCs based on P3HT-grafted MWNTs.

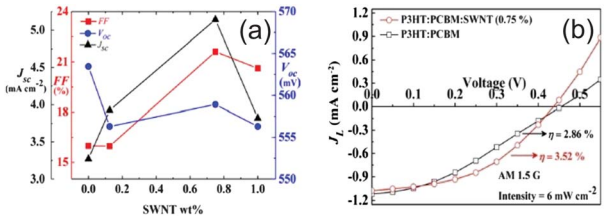

Fig. 7 Incorporating SWNTs into P3HT:PCBM BHSCs enhanced the PV performance. (a) PV characteristics dependence on SWNT concentration. (b) *I–V* curves of BHSCs with and without SWNTs under 6 mWcm^{-2} illumination. (Reprinted with permission from ref. 93. Copyright 2011, American Institute of Physics.)

In BHJ OPV, the electron or hole mobility can be selectively enhanced by incorporating N-doped MWNTs or B-doped MWNTs in active layers as demonstrated by electron-only and hole-only devices.[96] The enhanced charge transport was analyzed by PL emission and ultraviolet photoelectron spectroscopy (UPS) measurements, revealing that the work function of N-doped and B-doped MWNTs matched well with the LUMO of PCBM and the HOMO of P3HT, respectively. In BHSCs based on P3HT:PCBM, the PCE was increased from 3.0% in a reference cell without MWNTs to 4.1% by mixing B-doped MWNTs (1 wt%) in active layers, as shown in Fig. 8. The PV enhancement caused by B-doped MWNTs was more significant than undoped MWNTs, N-doped MWNTs and the mixture of B-doped and N-doped MWNTs, which was due to the balanced electron and hole mobilities (1.3×10^{-3} cm^{2}V^{-1}s^{-1} for electrons and 1.6×10^{-3} cm^{2}V^{-1}s^{-1} for holes) in active layers with B-doped MWNTs.[5–7] Meanwhile, due to an electrostatic repulsion among adjacent MWNTs doped by B or N, the dispersibility of CNTs was improved obviously as evaluated by optical microscopy images.

In the P3HT/SWNTs blend, CNTs provide nanosubstrates for the bconjugated polymer to crystallize.[54] Increased crystallinity of conjugated polymer has been observed in the X-ray diffraction (XRD) spectra of SWNTs-doped P3HT:PCBM blend films.[97] The additional reflection peak compared to those of P3HT:PCBM-only reference films indicated the existence of a higher crystallization degree of conjugated polymer domains and enhanced π–π stacking between benzene rings. Small-angle X-ray scattering (SAXS) results of P3HT/PCBM/SWNTs composites showed that the lamellar arrangement of the conjugated polymer was greatly improved due to SWNT addition.[98]

Given the excellent electrical properties and the solution processability, it is interesting to test the feasibility of graphene sheets in OPV applications.[99–104] The first BHSCs incorporating functionalized graphene as acceptor materials were fabricated based on the active layer of P3HT/phenyl isocyanate-treated GO blend, demonstrating a PCE of 1.1%.[42,43] By replacing P3HT

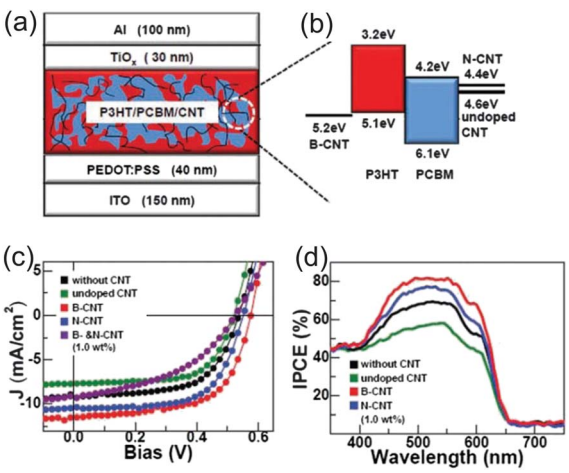

Fig. 8 PCE enhancement in OPV by doped and pristine MWNTs. (a) Schematic and (b) energy band diagram of the BHSCs. (c) *I–V* curves and (d) IPCE spectra of solar cells based on different CNTs conditions. *I–V* curves were tested under AM 1.5 100 mWcm^{-2} illumination. (Reprinted with permission from ref. 96. Copyright 2011 John Wiley and Sons.)

with alternative conjugated polymer P3OT, a higher PCE of 1.4% was achieved with the same device structure.[105] In these devices, functionalized graphene, which is soluble in common organic solvents, was synthesized by grafting phenyl groups onto GO. The GO can be obtained by the modified Hummers method.[106] The PL of conjugated polymer was significantly quenched after incorporation of functionalized graphene sheets, indicating that the photogenerated exciton in organic semiconductors could dissociate efficiently at the interfaces with graphene sheets by electron transfer from the conjugated polymer donor to the graphene acceptor.[43,44,105,107] A graphene weight fraction of 10% was found to be optimal for building an acceptor interpenetrating network in blend films. Less graphene content led to poor percolation connection, while a higher content ratio resulted in detrimental aggregates.[43] Functionalized MWNTs were incorporated in P3HT/GO BHSCs, yielding a PCE of 1.05%.[108] It was suggested that the addition of MWNTs in P3HT/GO blend films provided efficient electron transfer pathways, while the percolative GO network enhanced the hole transport. In P3HT:PCBM (1 : 1, w/w) BHSCs, the introduction of GO with optimized weight fraction led to a remarkable PCE increase from 0.88% to 1.4%.[109] GO thin film was utilized in P3HT:PCBM OPV devices acting as a hole-transporting and electron-blocking layer, demonstrating the similar functionality and comparable performance as PEDOT:PSS layer which is commonly used in OPV and OLED devices.[110]

Electronic interaction between GO and covalently grafted P3HT was confirmed to be stronger than that of the simple blend of these two materials. In ITO/PEDOT:PSS/P3HT grafted GO/C_{60}/Al bilayer solar cells, two-fold PCE improvement compared with that of the control device without covalent bonding was obtained.[111] Monosubstituted C_{60} molecules were grafted onto graphene by lithiation reaction. BHSCs with C_{60} grafted graphene sheet as acceptor and P3HT as donor exhibited a PCE of 1.22%,[112] as depicted in Fig. 9. This PCE was higher than that of the C_{60}:P3HT-only BHSCs (0.47%), because graphene sheets provided two dimensional electron transport pathways, greatly reducing the possibility of charge recombination during electron hopping among C_{60} molecules. The reference cells based on a C_{60}:graphene:P3HT blend without covalent bonding presented a PCE of only 0.44%, which was attributed to the poor interfacial contact between C_{60} and graphene sheets. In order to circumvent the undesirable modification of GO's electrical properties by the covalent grafting method, a novel noncovalent surfactant-assisted approach using didodecyldimethylammonium bromide (DDAB) as surfactant was developed to transfer GO from an aqueous phase to organic solution in order to make blend solutions with conjugated polymers.[113] OPV devices based on blend films of P3HT and noncovalently functionalized GO showed improved photoresponse.

By studying the fluorescence quenching and time-resolved fluorescence dynamics of the conjugated polymer/reduced graphene oxide sheets (RGO) mixture, two physical models were proposed to describe the energy transfer mechanism in the blend films.[114] The first model was based on Förster resonance energy transfer (FRET) to the randomly distributed defects on graphene, while the other model assumed that the excited donors were surrounded by a quasi-two-dimensional graphene network and ~5 nm was estimated to be the critical radius for effective energy transfer between conjugated polymer and graphene. The charge carrier transport mechanism in P3HT/RGO blend layers was further studied in TFT devices,[115] which is illustrated in Fig. 10. The hole mobility was increased significantly while the electron mobility remained unchanged. The graphene embedded in continuous P3HT films acted as short pathways for charge carrier transport, which reduced the effective channel length, resulting in enhanced hole mobility. KPFM measurements demonstrated that the charge injection barrier between P3HT and graphene was insignificant compared with the one presented at the source–drain contact, indicating good charge transport in the blend films.

Graphene quantum dots (GQDs) as new emerging zero dimensional nanocarbon materials have many advantageous properties for high efficiency BHSCs, such as large surface to volume ratio, high mobility and tuneable band gap. Functional GQDs with a uniform size of ~3–5 nm were obtained by a newly

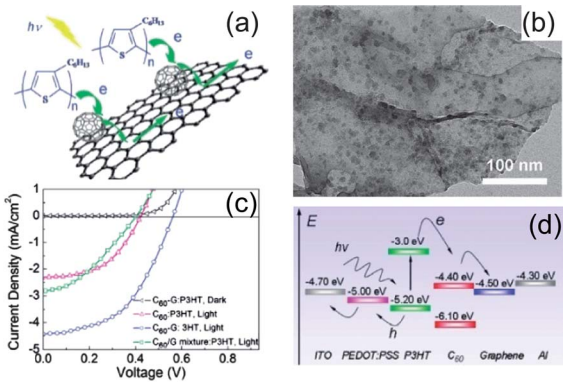

Fig. 9 BHSCs with the structure of ITO/PEDOT:PSS/P3HT:C_{60}-grafted graphene/Al demonstrated a PCE of 1.22%. (a) Schematic of the electron transfer mechanism in the active layers. (b) TEM of C_{60} grafted to graphene sheets. (c) *I–V* curves of solar cells with P3HT/C_{60}-grafted graphene, the P3HT/C_{60}, and the mixture of P3HT/C_{60}/graphene as active layers. (d) Energy band diagram of the BHSCs. (Reprinted from ref. 112 with permission. Copyright 2010 American Chemical Society.)

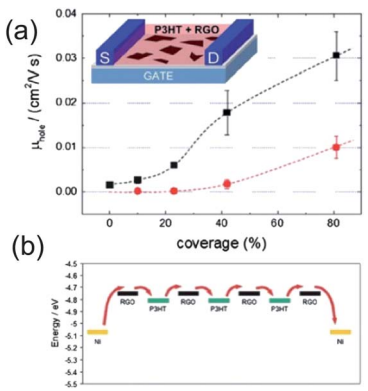

Fig. 10 Increased mobility was observed in P3HT/RGO films. (a) The hole mobility dependence on area coverage for RGO (red circles) and P3HT/RGO blend (black squares). (b) Schematic of the proposed charge transport mechanism in TFT devices. (Reprinted from ref. 115 with permission. Copyright 2011 The Royal Society of Chemistry.)

developed electrochemical method,[21] as shown in Fig.11. The as-synthesized GQDs had green PL and evaluated LUMO level at 4.2–4.4 eV. The measured V_{oc} of 0.77 V was close to the theoretical maximum (0.8 V) estimated by the difference between HOMO of P3HT and LUMO of GQDs. BHSCs based on P3HT and graphene QDs presented a PCE of 1.28%, demonstrating the feasibility for solution processed OPV applications. GQDs with an average diameter of ~9 nm were synthesized by an alternative hydrothermal approach,[22] as shown in Fig. 12. Aniline functionalized GQDs were blended with P3HT with different weight fractions, and PCE of 1.14% was achieved. The LUMO and HOMO of GQDs were 3.55 eV and 5.38 eV respectively, as measured by cyclic voltammetry (CV), indicating a favourable contact between GQDs and the aluminium cathode. A type II heterojunction was formed at the interface between P3HT and GQDs in the blend film, which is advantageous for OPV applications.

2.2 OPV based carbon nanomaterials/oligomers or small molecules

Blends of CNTs and conjugated oligomers or small molecules are also utilized as building blocks in OPV devices. Aided by conjugated pyrene moieties, oligothiophene was non-covalently assembled around SWNTs without altering the chemical structure of SWNT cores.[116] Conjugated oligomer 2,7-bis(3,3‴-didodecyl-[2,2′,5′,2″;5″,2‴]quaterthiophen-5-yl)-fluoren-9-one (QTF12) was blended with PCBM and double-walled carbon nanotubes (DWNTs) to fabricate BHSCs, showing a PCE of 0.43%.[117] The composites of protonated porphyrin (H_4P^{2+}) and SWNTs on nanostructured SnO_2 were applied as photoelectrodes in photochemical (PEC) solar cells, presenting an IPCE as high as ~13%.[118] SWNTs were functionalized by attachment of ZnPc derivatives to build photoelectrodes in PEC solar cells. A

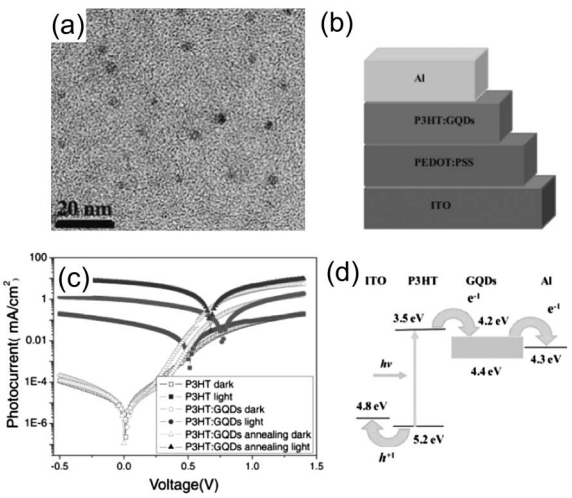

Fig. 11 BHSCs based on the blend of free standing GQDs and P3HT with a promising PCE of 1.28%. (a) TEM image of as-synthesized GQDs. (b) Schematic device structure of BHSCs. (c) *I–V* curves of reference cell (squares), P3HT/GQDs PV devices with (triangles) and without annealing (circles) process. (d) Energy level diagram of ITO/P3HT:GQDs/Al BHSCs. (Reprinted with permission from ref. 21. Copyright 2011 John Wiley and Sons.)

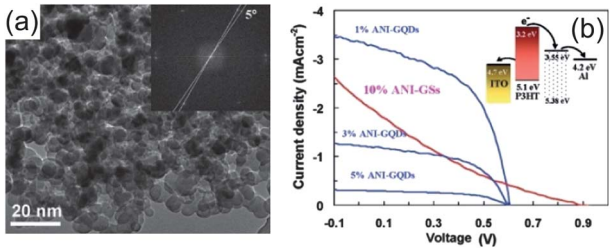

Fig. 12 GQDs as acceptor materials in BHSCs exhibiting a PCE of 1.14%. (a) TEM image of GQDs. Inset shows the fast Fourier transform (FFT) of GQDs, confirming that most GQDs are composed of 1 to 2 monolayers. (b) *I–V* curves of PV devices employing graphene sheets and aniline functionalized GQDs (ANI-GQDs) with different GQD contents, under AM 1.5 at 100 mWcm^{-2}. Inset shows the band diagram of BHSCs. (Reprinted from ref. 22 with permission. Copyright 2010 American Chemical Society.)

monochromatic IPCE as large as 17.3% was achieved.[119] The promising results suggested efficient photogenerated charge separation and transport processes in the composite of CNTs and small molecules, which were also identified by transient absorption results.[120]

A range of small organic molecules were decorated onto chemical modified graphene nano-sheets to study the PV characteristics of the composites. Photodetectors based on composites of RGO and water soluble CuPc derivative presented enhanced photoresponsivity compared with graphene-only devices because of efficient dissociation of photogenerated carriers at the large area of donor–acceptor interfaces.[121] Porphyrin antennae molecules were successfully anchored onto GO, and the active layer was coated on a transparent electrode by electrophoretic deposition, demonstrating an IPCE of 1.3% in a standard PEC solar cell,[122] as demonstrated in Fig. 13. In the blend photoelectrode, the photoexcited porphyrin antennae molecule rapidly returned to the ground state by transferring an electron to GO sheets. The captured electron could be efficiently collected by the electrode aided by the delocalized percolation network of GO.

The formation of a ground-state complex of chemically reduced GO and a water-soluble tetracationic porphyrin (TMPyP) in solution was inferred by the red-shifted absorption

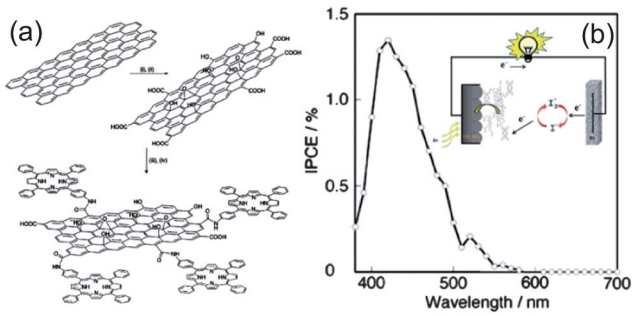

Fig. 13 Porphyrin antennae molecules anchored on GO as photoelectrode in PEC solar cells. (a) Schematic of porphyrin decoration. (b) IPCE spectrum of the photoelectrode. Inset shows the PEC cell measurement setup. (Reprinted from ref. 122 with permission. Copyright 2011 The Royal Society of Chemistry.)

peak of porphyrin.[123] The reduction of porphyrin fluorescence lifetime and transient absorption measurement results indicated strong electronic interactions between graphene and absorbed TMPyP molecules, which was further confirmed by the detected charge separation processes at the TMPyP–graphene interface in PEC solar cells. Similar photocurrent enhancement was also observed in GO/phthalocyanine blend films.[124] The photoresponse of an active layer comprising of butylamine modified graphene sheets and bisphenazine discoid molecules 2,11-di-*tert*-butyl-6,7,15,16-tetrakis(hexylthio)quinoxalino[2′,3′:9,10]phenanthro[4,5-*abc*]phenazine (TQPP) was stronger than the blend film without graphene amine-modification, which was probably attributed to the homogenous film morphology cast from better dispersed amine-treated blend solution.[125]

Table 1 summarizes the OPV performance based on carbon nanomaterials and organic components under simulated air mass (AM) 1.5 illumination at 100 mWcm^{-2}.

3. Silicon-based HSCs and OPV

Silicon is the dominant inorganic material in the semiconductor industry due to its excellent electronic properties, non-toxic nature, stability and abundance on earth. Single crystalline and micro-crystalline silicon solar cells share ~80–90% of the commercial solar cell market. The highest PCE of single junction silicon solar cells reached ~25% in 2008, as announced by Martin Green's group. This PCE is close to the ~29–31% theoretical maximum of first-generation solar cells based on crystalline silicon wafers, indicating the already highly optimized fabrication condition of traditional silicon solar cells. One of the main obstacles limiting large-scale PV application is the expensive price of solar panels due to the use of high quality silicon wafers and the cost of complicated fabrication processes. The incorporation of nanotechnology is expected to introduce further improvements in silicon based solar cells, such as enhanced light trapping ability, hot carrier collection and multiple exciton generation (MEG) effects. One dimensional SiNW arrays with high aspect ratio allow efficient light harvesting using less silicon material compared to planar wafers. The radial charge transfer path also benefits the PV performance in core-shell structured SiNW solar cells.[29,126,127] Several methods have been developed to fabricate large-scale high-quality SiNW arrays, including Ag ion-assisted solution etching,[128,129] reactive ion etching (RIE),[130–133] metal nanoparticle (NP) catalyzed vapour-liquid-solid (VLS) chemical vapour deposition (CVD).[134–137] SiNWs provide large surface area, exhibiting excellent catalytic performance in

Table 1 Summary of OPV based on carbon nanomaterials and organic components under simulated AM 1.5 illumination at 100 mWcm^{-2}

Device structure	J_{sc} (mAcm^{-2})	V_{oc} (V)	FF	PCE (%)	Reference
ITO/P3OT:SWNTs/Al	0.2	0.75	0.4	0.06	53
ITO/P3OT:dye-SWNTs/Al	0.18	0.6	0.35	0.036	77
ITO/MWNTs:PTEBS/C_{60}/Al	1.49	0.62	0.61	0.56	64
ITO/PEDOT:PSS/P3HT:C_{60}-SWNTs/Al	2.72	0.386	0.512	0.57	78
ITO/PEDOT:PSS/ P3HT:PCBM:MWNTs/LiF/Al	9.3	0.57	0.384	2.0	86
ITO/PEDOT:PSS/P3HT:PCBM:SWNTs/ Al	4.95	0.55	0.52	1.4	87
ITO/PEDOT:PSS/ QTF12:PCBM:DWNTs/LiF/Al	2.45	0.53	0.33	0.43	117
ITO/PEDOT:PSS/ P3HT:PCBM:MWNTs/Al	11.33	0.52	0.546	3.47	91
ITO/PEDOT:PSS/P3HT-MWNTs/C_{60}/ Ca/Al	2.2	0.38	0.35	0.29	94
ITO/PEDOT:PSS/P3HT:PCBM:SWNTs/ LiF/Al	11.14	0.668	0.522	3.66	97
ITO/PEDOT:PSS/P3HT:PCBM:B-doped MWNTs/TiO_x/Al	11.47	0.57	0.613	4.1	96
ITO/P3HT:PCBM:thiophene-MWNTs/ BCP/Al	6.49	0.62	0.62	2.5	89
ITO/PEDOT:PSS/P3HT:phenyl-graphene/LiF/Al	4.2	0.92	0.37	1.4	105
ITO/PEDOT:PSS/P3HT:phenyl-graphene/LiF/Al	4.0	0.72	0.38	1.1	42,43
ITO/PEDOT:PSS/P3HT:PCBM:phenyl-graphene/LiF/Al	5.3	0.64	0.41	1.4	109
ITO/PEDOT:PSS/P3HT:phenyl-graphene/LiF/Al	3.72	0.77	0.31	0.88	44
ITO/PEDOT:PSS/amine-graphene/ P3HT:PCBM/LiF/Al	3.26	0.556	0.41	0.74	46
ITO/GO/P3HT:PCBM/Al	11.4	0.57	0.543	3.5	110
ITO/PEDOT:PSS/ P3HT:MWNTs:phenyl-graphene/LiF/Al	4.7	0.67	0.32	1.05	108
ITO/PEDOT:PSS/P3HT-graphene/C_{60}/Al	3.5	0.43	0.41	0.61	111
ITO/PEDOT:PSS/P3HT:aniline-GQDs/ LiF/Al	3.51	0.61	0.53	1.14	22
ITO/PEDOT:PSS/P3HT:GQDs/Al	6.33	0.67	0.3	1.28	21
ITO/PEDOT:PSS/C_{60}-graphene:P3HT/Al	4.45	0.56	0.49	1.22	112

hydrogen generation by splitting water.[138] The optoelectrical properties have been investigated in PV devices based on either single SiNW,[139,140] or SiNW arrays.[28,141–151] Because the minority carrier transfer distance is greatly reduced in core-shell structured SiNW solar cells, cheaper silicon wafers with lower mobility could be potentially used to achieve high-performance nano-structured solar cells and effectively reduce the fabrication cost.[152,153] The theoretical model predicts that devices with a PCE greater than 15% can be obtained in radial junction structured silicon solar cells using silicon material with a minority carrier length less than 10 μm.[126] However, the p–n junctions in these SiNW array solar cells are mostly formed by high-temperature (950 °C) dopant diffusion processes, which represents a certain portion of the fabrication cost and shortens the lifetime of minority charge carriers in the presence of metal impurities. Solution-processed techniques are commonly used in synthesizing and processing of both organic semiconductors and inorganic nanomaterials. By depositing organic materials or inorganic semiconductor NCs onto the surfaces of planar silicon substrates, heterojunctions can be formed, showing promising PV performances.[154–163] HSCs based on SiNW arrays fabricated by simple and cheap fabrication processes should be technological alternatives for the present commercial silicon solar cells.

3.1 Solar cells based on silicon nanostructures and polymers

Solution-processable conjugated polymers are commonly used organic materials to construct OPV and HSCs with nanostructured silicon substrates. The good dispersion in ordinary organic solvents allows the deposition of a uniform organic layer closely wrapped on the surfaces of textured silicon substrates. Bilayer heterojunction HSCs made by casting the conjugated polymer MEH:PPV onto a laser-textured surface of amorphous silicon film deposited on ITO glass presented a PCE of 0.87%.[164] HSCs based on the organic-inorganic p–n heterojunction of electrochemically deposited *p*-poly(3-methylthiophene) (*p*-PMeT) on alkaline solution-textured silicon substrates were fabricated, exhibiting a PCE of 0.42%.[165] Absorption of infrared light by organic materials and subsequent exciton transfer to SiNWs *via* FRET are predicted and experimentally demonstrated by detecting a 60% increment of photocurrent from a silicon layer covered by the donor polymer MEH:PPV.[166] Textured amorphous silicon nanocone arrays on ITO were fabricated by PECVD deposition and subsequent RIE treatment masked by poly(styrene-*block*-methyl methacrylate) (PS-*b*-PMMA) diblock copolymer,[167] as illustrated in Fig. 14. Then the blend of P3HT:PCBM was deposited onto the as-made nanotextured substrates to prepare BHSCs. It was found that a PEDOT:PSS conducting layer between the inorganic nanostructures and organic blend films led to partial recombination of electrons and holes, effectively bridging the charge carrier transfer through the organic-inorganic interfaces. In comparison with conversional OPV devices with ITO/PEDOT:PSS/P3HT:PCBM/Al structure, the V_{oc} increased from 0.51 to 0.78 V and the PCE increased from 1.73% to 2.22% in these BHSCs based on silicon nanostructures. These studies verified the validity and advantages of conjugated polymer/nanostructured silicon heterojunction in PV devices.

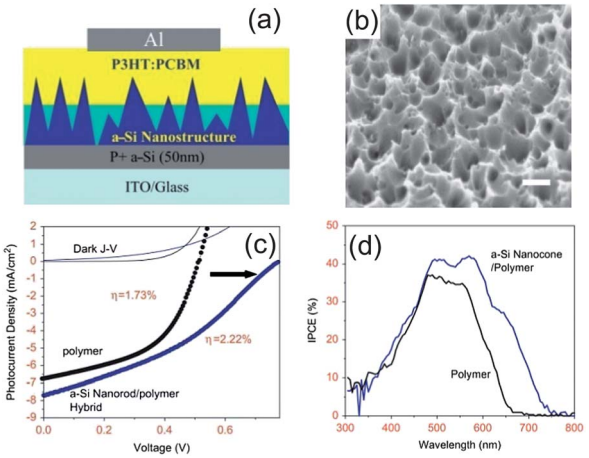

Fig. 14 BHSCs with ITO/p$^+$ a-Si/a-Si nanostructure/PEDOT:PSS/P3HT:PCBM/Al structure showed a PCE of 2.22%. (a) Schematic of device structure. (b) SEM image of nanostructured a-Si surface on ITO substrate. (c) *I–V* characteristics in the dark and under AM 1.5 light and (d) IPCE spectra of solar cells with and without silicon nanostructures. (Reprinted from ref. 167, Copyright 2011, with permission from Elsevier.)

SiNW arrays are supposed to give better performance since the light trapping effects and large surface area outperform these textured silicon surfaces manufactured by traditional techniques. In typical synthesis methods, as-made SiNW arrays are usually standing vertically on planar substrates like ITO glasses or silicon wafers. To exclusively study the intrinsic PV properties of SiNW arrays, it is required to peel SiNWs off from the mother substrates and transfer them to a specific location to construct functional devices. Successful transferring methods were developed using polymers as supporting matrix.[168–170] The polymer supported SiNW arrays grown by the VLS method act as efficient photoelectrodes in PEC solar cells, experimentally demonstrating the unique advantages of SiNWs in PV applications.

BHSCs based on P3HT:PCBM blends and solution-etched SiNW arrays were fabricated by pressing the n-type SiNWs substrates onto the polymer blend at elevated temperature above the glassy transition temperature of conjugated polymer and applying a lateral force after the hybrid system cooled down.[171] SiNW arrays in P3HT:PCBM BHJ blends enhanced the optical absorption and electron transport in the BHSC. And the dissociation of excitons was also improved due to the increase of additional junction area between P3HT and SiNWs, which finally led to over 50% improvement of PCE from 1.21% to 1.91%. In typical BHSCs, ITO is used as the anode, while the deposited Al electrode acts as the cathode.[172] Recently, ITO coated with an electron-transport, hole-blocking layer, usually ZnO, is frequently employed as the cathode in BHSCs presenting stable and impressive PCE.[173,174] Since the polarity is opposite to the normal BHSC configuration, the device structure with an ITO cathode is defined as an inverted structure in BHSCs. BHSCs with inverted structure were constructed using VLS grown p-type SiNW arrays on ITO substrates.[175] The blend of P3HT and PCBM was spin coated onto as-prepared SiNW array substrates. The PV characterization indicated that the SiNW arrays could act as both a photoactive hole-transporting layer

when Al electrode was used in normal BHSC geometry, and a charge dissociation electron-transfer layer using gold as the anode in the inverted structure. PV devices based on a 1 : 1 (w/w) blend of P3HT/MWNTs instead of commonly used P3HT:PCBM were fabricated by drop casting these mixtures onto solution-etched n-type SiNW arrays. The resulting PCE of 0.61% was three times larger than those of the devices without CNTs.[176]

The PCEs of these previously reported PV devices are still much lower than those of commercial silicon solar cells. There are three main issues limiting the ultimate PCE: first, the increased density of surface traps in SiNWs induced by large surface area and defects during synthesis processes acting as recombination centres for photo-generated charge carriers, leading to low efficiency; second, the relatively lower mobility of organic semiconductors compared to silicon hampers the charge separation and transport by mechanisms such as tunnelling-enhanced recombination and space-charge-limited current (SCLC);[157] third, organic materials with large absorption coefficient block a considerable amount of light from reaching SiNWs if the organic layer is too thick. In order to passivate the surface traps in SiNWs to reduce recombination, amorphous silicon was deposited on the surface of a single SiNW as a shell layer by the VLS method.[139] *In situ* measurements revealed that the surface recombination was reduced by nearly 2 orders of magnitude, and more than 90-fold higher photoresponse was obtained in the passivated SiNW compared with the bare silicon core. By applying an amorphous silicon passivation layer in SiNW arrays, a PCE as high as 11.0% has been achieved.[177,178] Organic functionality termination of a silicon surface could significantly reduce the surface recombination velocity.[179] By converting the Si–H bonds into Si–C ones in SiNW arrays *via* a two-step chlorination/methylation process, the charge recombination at the silicon–conjugated polymer interface was effectively suppressed, and a much larger PCE of 5.9% was demonstrated,[180] which is illustrated in Fig. 15. In designing the HSC structure, the thickness of the organic semiconductor layer should be as thin as possible if it can form a continuous film on the SiNW shell. The fabricated solar cell presented an inorganic–organic core-shell structure with SiNW cores and P3HT shells, instead of the embedded structure with the SiNW array immersed in a thick polymer matrix. In this way, the light absorption by the organic layer was greatly reduced, and simultaneously, the short exciton diffusion length and limited charge carrier transport problems in the conjugated polymer layer were alleviated due to the ultra-thin film.[181] The introduction of electrochemically deposited Pt NPs at the SiNW array surface yielded substantial improvements of PCE in PEC solar cells, which was caused by the formation of a Pt-Si junction and the catalytic activity of Pt NPs.[182] In the conjugated polymer/SiNW HSCs, the decoration of Pt NPs led to more than 70% enhancement of PCE compared with the control device without Pt NPs. Pt NPs played two critical roles in modifying the organic–inorganic interfaces: on the one hand, Pt NPs tended to nucleate at the Si–H bonding areas where methyl groups were absent, which substantially decreased the surface recombination velocity; on the other hand, revealed by UPS results, the build-in potential at the SiNW surfaces was increased for favourable separation of photogenerated carriers.

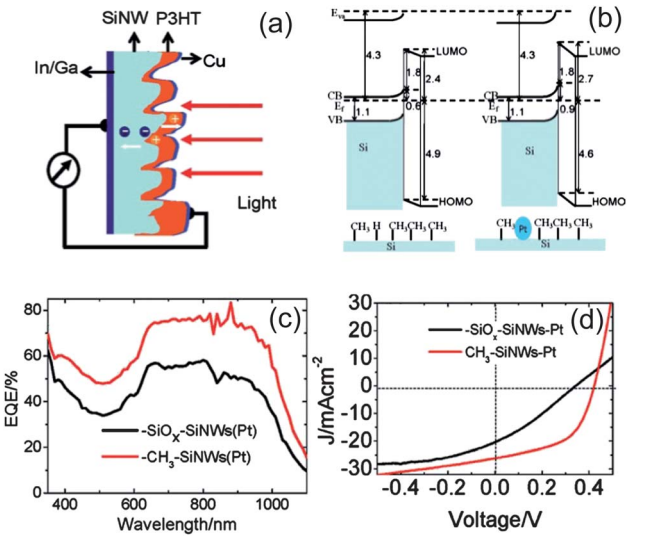

Fig. 15 High-efficiency conjugated polymer/SiNW core-shell structured HSCs with the structure of semitransparent Cu/P3HT/Pt NPs decorated CH_3-SiNW array/In:Ga. (a) Schematic of device structure. (b) Band diagram before and after Pt NP decoration. (c) EQE and (d) *I–V* curves of devices with methyl groups or silicon oxide passivation. (Reprinted from ref. 180 with permission. Copyright 2011 American Chemical Society.)

The conductive polymer PEDOT:PSS is another remarkable organic material widely used in OPV and OLED devices as hole transporting layer. HSCs employing PEDOT:PSS as the organic counterpart fabricated by pressing n-type SiNW array substrates onto a wet PEDOT:PSS film cast on ITO exhibited stable rectifying diode behaviour and promising PV performance.[183] The work function of PEDOT:PSS is 5.1 eV, close to the valence band of silicon, indicating the absence of injection barriers in the hybrid junction. Compared with PEDOT:PSS/planar silicon substrate bilayer devices, the series resistance was much lower due to the larger junction area in SiNW based devices. Meanwhile, the strong light trapping effect in SiNW array devices reduced the reflection substantially, which boosted the J_{sc} from 1.27 to 19.28 mAcm^{-2}, and the PCE from 0.08% to 5.09%. By further tuning the morphology of SiNW arrays, a higher PCE of 5.14% was obtained.[184]

In planar metal/silicon Schottky devices, the V_{oc} is usually lower than the theoretical maximum, which is caused by the Fermi level pinning effect at the metal/silicon interfaces. However, in PEDOT:PSS/SiNW HSCs fabricated with soft solution processed techniques, V_{oc} as high as 0.62 V was detected, indicating the absence of Fermi level pinning and effective passivation of the organic–inorganic interfaces.[185] HSCs based on SiNW arrays embedded in a thick PEDOT:PSS layer exhibited a PCE of 5.3%.[186] In the PEDOT:PSS/SiNW solar cells with core-shell structure, the PCE was further improved to 6.35%,[187] as shown in Fig. 16. In a recent report, PCE as high as 9% has been achieved by optimizing the length of SiNWs.[188] The analysis of dark current characteristics in these devices revealed that the interfacial recombination of charge carriers was the bottle-neck of PV performances. The incorporation of proper SiNW surface passivation and hole-transporting electron-blocking layer was suggested to be

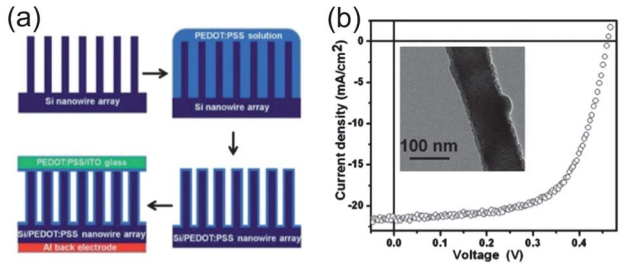

Fig. 16 PEDOT:PSS-SiNW array core-shell structured HSCs demonstrated a PCE of 6.35%. (a) Schematic of the PV device fabrication steps. (b) *I–V* characteristics under AM 1.5 at 100 mWcm^{-2}. Inset is the TEM image of an individual core-shell structure. (Reprinted from ref. 187 with permission. Copyright 2011 The Royal Society of Chemistry.)

beneficial to the PCE. Inferred from the *I–V* responses of silicon heterojunction with either gold or PEDOT:PSS contacts under various conditions, it was revealed that the velocity of majority carrier charge transfer in the polymer/silicon contact was several orders lower than at the metal/silicon contact. The low velocity of majority carrier at the organic–inorganic interface was coincident with the excellent PV performance of these HSCs.[189]

3.2 Silicon/small molecules HSCs

Given the advantages of silicon nanostructures in PV applications, organic small molecules were surveyed to construct novel hybrid devices in combination with silicon.[190–195] Increased light-induced conductance caused by electron tunnelling from organic molecules to silicon was identified in lateral SiNW FET devices coated with a porphyrin derivative.[193] In PEC solar cells with a porphyrin derivative sensitized SiNW array as the photoelectrode, a photocurrent peak in the near infrared region was observed, which indicated the presence of direct interfacial charge transfer between the HOMO of organic molecules to the conduction band of SiNW arrays.[194] Solar cells with the hybrid structure of ZnPc/gold NPs/ultrathin silicon dioxide/nanoporous textured silicon substrates were prepared. The nanotextured silicon was formed by RIE treatments employing anodic aluminium oxide as a mask, and a PCE of 4.9% was obtained.[196] Organic hole-transporting material 2,2′,7,7′-tetrakis(*N*,*N*-di-4-methoxyphenylamino)-9,9′-spirobifluorene (spiro-OMeTAD) was deposited on SiNW arrays to fabricate core-shell structured HSCs.[197] The observed PCE of 10.3% established a PCE record for HSCs based on heterojunctions of organic small molecule/SiNW arrays. The devices configuration can vary from core-shell structure to embedded geometry by controlling the density of the SiNW array and the thickness of the spiro-OMeTAD layer,[198] as demonstrated in Fig. 17. The core-shell structured device presented better PV performance than the embedded one due to the efficient charge transport and less optical loss in the thin organic shell. An additional PEDOT:PSS layer between spiro-OMeTAD and the metal electrode resulted in a higher V_{oc} than the reference cell without PEDOT:PSS, because of improved electrical contact. By further optimizing the PEDOT:PSS buffer layer and the thickness of the organic film, the PCE reached 9.7%.

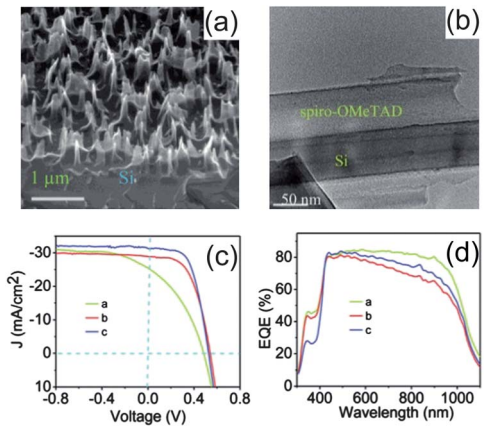

Fig. 17 Core-shell and embedded structured HSCs based on spiro-OMeTAD and SiNW arrays. (a) SEM and (b) TEM images of hybrid core-shell structures. (c) *I–V* curves and (d) EQE spectra of core-shell HSCs with different configurations: a. In:Ga/SiNWs/spiro-OMeTAD/Cu:Ag (green); b. In:Ga/SiNWs/spiro-OMeTAD/PEDOT:PSS/Cu:Ag (red); c. In:Ga/SiNWs/spiro-OMeTAD/Cu/PEDOT:PSS/Cu:Ag (blue). *I–V* curves were measured under AM 1.5 illumination at 100 mWcm^{-2}. (Reprinted from ref. 198 with permission. Copyright 2011 American Chemical Society.)

3.3 BHSCs based on free standing Si nanostructures

Free standing Si NCs have attracted wide interest in recent years, owning to their distinct optical and electrical properties,[199–203] compatibility with the mature silicon fabrication technology,[204] and the potential application in MEG solar cells.[205,206] The feasibility of s-SWNTs/Si NC BHSCs was demonstrated with a preliminary PCE of 0.01%.[207] Schottky photovoltaic devices were constructed based on solution-processed Si NC films with the simple structure of ITO/Si NCs/Al. The obtained PCE of 0.02% verified the PV effect of Si NPs.[208] Bilayer heterojunction solar cells with the structure of ITO/PEDOT:PSS/Si NCs/C_{60}/Al demonstrated an IPCE of 1.4% at the short wavelength range.[209]

As studied *via* light-induced electron spin resonance (LESR), a favourable band alignment between Si NCs and P3HT for efficient exciton dissociation was identified, indicating the feasibility of using a P3HT/Si NC blend as the photoactive layer in OPV applications.[210] Hybrid BHSCs based on blend films of Si NCs/P3HT exhibited J_{sc} of 3.3 mAcm^{-2}, V_{oc} of 0.75 V and FF of 0.46, yielding a PCE of 1.15%.[23] The optimal Si NCs/P3HT weight ratio was from 30% to 70%, which enabled the formation of a percolative inorganic NC network for electron transfer,

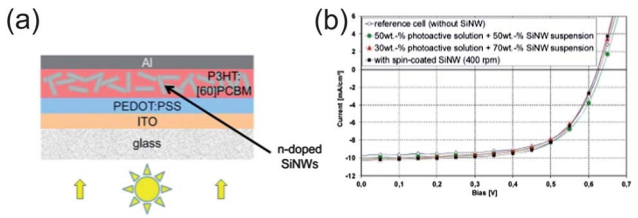

Fig. 18 SiNWs distributed in a P3HT:PCBM active layer as an efficient electron transporter. (a) Schematic of device structure. (b) *I–V* curves of P3HT:PCBM-based OPV with and without SiNWs. (Reprinted from ref. 214 with permission. Copyright 2011 Institute of Physics.)

Table 2 Summary of HSCs and OPV based on silicon nanostructures and organic components under simulated AM 1.5 illumination at 100 mWcm^{-2}

Device structure	J_s (mA cm^{-2})	V_{oc} (V)	FF	PCE (%)	Reference
HSCs					
ITO/laser textured nc-Si:H/MEH-PPV/Al	6.65	0.56	0.23	0.87	164
ITO/PEDOT:PSS/ZnPc/GNPs/UT-SiO_2/porous Si	26.0	0.565	0.334	4.9	196
Cu/P3HT/Pt NP-CH_3-SiNWs/In:Ga	26.2	0.421	0.53	5.9	180
ITO/PEDOT:PSS/SiNWs	19.28	0.47	0.61	5.09	183
ITO/PEDOT:PSS/SiNWs	21.7	0.39	0.61	5.14	184
ITO/PEDOT:PSS/SiNWs/Al	21.6	0.46	0.64	6.35	187
Ag/PEDOT:PSS/SiNWs/Au	—	—	0.308	5.3	186
Ag/PEDOT:PSS/SiNWs/Al	26.3	0.53	0.642	9.0	188
Ag/PEDOT:PSS/spiro-OMeTAD/SiNWs/Al	30.9	0.57	0.588	10.3	197
Ag/Cu/PEDOT:PSS/Cu/spiro-OMeTAD/SiNWs/In:Ga	31.3	0.527	0.588	9.7	198
ITO/PEDOT:PSS/Si NCs:P3HT/Al	3.3	0.75	0.46	1.15	23
ITO/PEDOT:PSS/Si NCs:P3HT/Al	3.8	0.8	0.47	1.47	211
ITO/PEDOT:PSS/Si NCs:SWNTs/Al	0.3	0.14	0.25	0.01	207
OPV					
ITO/PEDOT:PSS/P3HT:Si NCs-MWNTs/Al	0.192	0.69	0.335	4.45×10^{-2}	213
ITO/PEDOT:PSS/P3HT:PCBM:SiNWs/Al	11.61	0.425	0.39	1.93	171
ITO/SiNWs/P3HT:PCBM/Al	5.25	0.259	0.313	0.427	175
Au/P3OT:MWNTs/SiNWs	7.85	0.353	0.22	0.61	176
ITO/p^+ a-Si/a-Si nanocones/PEDOT:PSS/P3HT:PCBM/Al	7.7	0.78	0.37	2.22	167
ITO/PEDOT:PSS/P3HT:PCBM:Si rods/Al	10.31	0.621	0.65	4.16	214

meanwhile, it retained a maximized interfacial area for exciton dissociation. By further optimizing the post-annealing treatments, the PCE was improved to 1.47%.[211] Photocurrent spectroscopy results indicated that the photocurrent came from both organic and inorganic counterparts, and the Si NCs could convert near infrared light unabsorbed by P3HT into additional current.[212] The PV characteristics revealed a potential barrier hampering the hole transfer from Si NCs to P3HT.[23] This disadvantageous band alignment between the silicon valence band and the HOMO level of P3HT could be eliminated by using smaller NCs with larger band gap due to more pronounced quantum confinement effects. Si NCs were covalently bonded onto the sidewalls of MWNTs to fabricate BHSCs based on a blend of P3HT/Si NCs-MWNTs. Compared with devices using only Si NCs or only MWNTs as acceptors, significant PCE improvements were obtained, which was attributed to efficient exciton dissociation at P3HT/Si NC interfaces and facilitated charge transport by MWNTs.[213] Dispersions of free standing SiNWs were obtained by sonication of SiNW arrays in chlorobenzene.[214] Adding as-prepared SiNWs into P3HT:PCBM BHSCs as electron transport short pathways led to an improved PCE of 4.2% compared with the reference cell without SiNW addition, as shown in Fig. 18.

The PV performance of HSCs and OPV based on silicon nanostructures and organic components under simulated AM 1.5 illumination at 100 mWcm^{-2} is summarised in Table 2.

4. Summary and outlook

Solar cells based on group IV nanostructures and conjugated organic materials have made rapid progress in recent years. The inorganic nanomaterials can be CNTs, graphene, SiNWs and free standing Si NCs. The organic counterparts are composed of conjugated polymers and photoactive small molecules. Two kinds of device geometries have been explored, namely, BHJ structure and three dimensional wire array structure. In BHSCs, CNTs, GO, free standing GQDs and Si NCs are applied as acceptor materials. By optimizing the surface chemistry modification and concentration of these inorganic nanostructures, percolative networks can be formed in the organic semiconductor matrix. These group IV nanomaterials demonstrate efficient exciton dissociation and charge carrier transport characteristics in PV applications. In addition, the nano-carbon material could enhance the crystallinity and mobility of a conjugated polymer leading to improved PV performance of BHJ OPV. SiNW arrays show excellent light trapping and charge transporting properties. The unique radial heterojunction formed between SiNWs and conjugated organic materials alleviate the short exciton diffusion length and low mobility drawbacks of organic materials. Especially, the PCE could be further enhanced in carefully designed core-shell structured HSCs based on ultra thin organic layers and SiNW arrays. The solution processed techniques and low-temperature compatible fabrication methods render these HSCs as promising candidates for high-performance and low-cost PV applications. By rationally modifying the group IV nanomaterials with functional groups, better surface passivation and optimized band alignment with organic materials are expected to further boost the PV performance.

Acknowledgements

This work was supported by the National Basic Research Program of China (973 Program) (Grant No. 2012CB932402), National Natural Science Foundation of China (Grant No. 60976050, 61176057, 91123005), Scientific Research Foundation for the Returned Overseas Chinese Scholars of State Education Ministry, the Priority Academic Program Development of Jiangsu Higher Education Institutions.

Notes and references

1 C. J. Brabec, N. S. Sariciftci and J. C. Hummelen, *Adv. Funct. Mater.*, 2001, **11**, 15.
2 C. W. Tang, *Appl. Phys. Lett.*, 1986, **48**, 183.
3 P. Peumans, S. Uchida and S. R. Forrest, *Nature*, 2003, **425**, 158.
4 J. J. M. Halls, C. A. Walsh, N. C. Greenham, E. A. Marseglia, R. H. Friend, S. C. Moratti and A. B. Holmes, *Nature*, 1995, **376**, 498.
5 J. J. Dittmer, R. Lazzaroni, P. Leclère, P. Moretti, M. Granström, K. Petritsch, E. A. Marseglia, R. H. Friend, J. L. Brédas, H. Rost and A. B. Holmes, *Sol. Energy Mater. Sol. Cells*, 2000, **61**, 53.
6 G. Li, V. Shrotriya, J. Huang, Y. Yao, T. Moriarty, K. Emery and Y. Yang, *Nat. Mater.*, 2005, **4**, 864.
7 M. M. Mandoc, L. J. A. Koster and P. W. M. Blom, *Appl. Phys. Lett.*, 2007, **90**, 133504.
8 S. Jeong, S.-H. Woo, H.-K. Lyu and Y. S. Han, *Sol. Energy Mater. Sol. Cells*, 2011, **95**, 1908.
9 Z. He, C. Zhong, X. Huang, W.-Y. Wong, H. Wu, L. Chen, S. Su and Y. Cao, *Adv. Mater.*, 2011, **23**, 4636.
10 S. Günes, H. Neugebauer and N. S. Sariciftci, *Chem. Rev.*, 2007, **107**, 1324.
11 W. J. E. Beek, M. M. Wienk and R. A. J. Janssen, *J. Mater. Chem.*, 2005, **15**, 2985.
12 Y. Kang and D. Kim, *Sol. Energy Mater. Sol. Cells*, 2006, **90**, 166.
13 N. C. Greenham, X. Peng and A. P. Alivisatos, *Phys. Rev. B: Condens. Matter*, 1996, **54**, 17628.
14 W. U. Huynh, J. J. Dittmer and A. P. Alivisatos, *Science*, 2002, **295**, 2425.
15 B. Q. Sun, E. Marx and N. C. Greenham, *Nano Lett.*, 2003, **3**, 961.
16 B. Sun, A. T. Findikoglu, M. Sykora, D. J. Werder and V. I. Klimov, *Nano Lett.*, 2009, **9**, 1235.
17 H. Fu, S.-W. Tsang, Y. Zhang, J. Ouyang, J. Lu, K. Yu and Y. Tao, *Chem. Mater.*, 2011, **23**, 1805.
18 D. Cui, J. Xu, T. Zhu, G. Paradee, S. Ashok and M. Gerhold, *Appl. Phys. Lett.*, 2006, **88**, 183111.
19 Y. Okada, R. Oshima and A. Takata, *J. Appl. Phys.*, 2009, **106**, 024306.
20 C. G. Bailey, *Appl. Phys. Lett.*, 2011, **98**, 163105.
21 Y. Li, Y. Hu, Y. Zhao, G. Shi, L. Deng, Y. Hou and L. Qu, *Adv. Mater.*, 2011, **23**, 776.
22 V. Gupta, N. Chaudhary, R. Srivastava, G. D. Sharma, R. Bhardwaj and S. Chand, *J. Am. Chem. Soc.*, 2011, **133**, 9960.
23 C.-Y. Liu, Z. C. Holman and U. R. Kortshagen, *Nano Lett.*, 2009, **9**, 449.
24 B. Sun, G. Zou, X. Shen and X. Zhang, *Appl. Phys. Lett.*, 2009, **94**, 233504.
25 I. Gonzalez-Valls and M. Lira-Cantu, *Energy Environ. Sci.*, 2009, **2**, 19.
26 J. J. Chao, S. C. Shiu, S. C. Hung and C. F. Lin, *Nanotechnology*, 2010, **21**, 285203.
27 J. R. Maiolo, B. M. Kayes, M. A. Filler, M. C. Putnam, M. D. Kelzenberg, H. A. Atwater and N. S. Lewis, *J. Am. Chem. Soc.*, 2007, **129**, 12346.
28 X. Shen, B. Sun, F. Yan, J. Zhao, F. Zhang, S. Wang, X. Zhu and S. Lee, *ACS Nano*, 2010, **4**, 5869.
29 K.-Q. Peng and S.-T. Lee, *Adv. Mater.*, 2011, **23**, 198.
30 D. Tasis, N. Tagmatarchis, A. Bianco and M. Prato, *Chem. Rev.*, 2006, **106**, 1105.
31 H. Ago, K. Petritsch, M. S. P. Shaffer, A. H. Windle and R. H. Friend, *Adv. Mater.*, 1999, **11**, 1281.
32 S. Reich, C. Thomsen and J. Maultzsch *Carbon nanotubes: basic concepts and physical properties*; Wiley, 2004.
33 T. Schuettfort, A. Nish and R. J. Nicholas, *Nano Lett.*, 2009, **9**, 3871.
34 V. Sgobba and D. M. Guldi, *J. Mater. Chem.*, 2008, **18**, 153.
35 R. A. Hatton, A. J. Miller and S. Silva, *J. Mater. Chem.*, 2008, **18**, 1183.
36 K. S. Novoselov, A. K. Geim, S. V. Morozov, D. Jiang, Y. Zhang, S. V. Dubonos, I. V. Grigorieva and A. A. Firsov, *Science*, 2004, **306**, 666.
37 A. K. Geim and K. S. Novoselov, *Nat. Mater.*, 2007, **6**, 183.
38 X. Xu, Q. Luo, W. Lv, Y. Dong, Y. Lin, Q. Yang, A. Shen, D. Pang, J. Hu, J. Qin and Z. Li, *Macromol. Chem. Phys.*, 2011, **212**, 768.
39 M. Castelain, H. J. Salavagione, R. Gomez and J. Luis Segura, *Chem. Commun.*, 2011, **47**, 7677.
40 D.-W. Lee, T. Kim and M. Lee, *Chem. Commun.*, 2011, **47**, 8259.
41 C. Valles, P. Jimenez, E. Munoz, A. M. Benito and W. K. Maser, *J. Phys. Chem. C*, 2011, **115**, 10468.
42 Q. Liu, Z. Liu, X. Zhang, N. Zhang, L. Yang, S. Yin and Y. Chen, *Appl. Phys. Lett.*, 2008, **92**, 223303.
43 Q. Liu, Z. Liu, X. Zhong, L. Yang, N. Zhang, G. Pan, S. Yin, Y. Chen and J. Wei, *Adv. Funct. Mater.*, 2009, **19**, 894.
44 Z. Liu, D. He, Y. Wang, H. Wu and J. Wang, *Sol. Energy Mater. Sol. Cells*, 2010, **94**, 1196.
45 Y. Xu, Y. Wang, J. Liang, Y. Huang, Y. Ma, X. Wan and Y. Chen, *Nano Res.*, 2009, **2**, 343.
46 L. Valentini, M. Cardinali, S. B. Bon, D. Bagnis, R. Verdejo, M. Angel Lopez-Manchado and J. M. Kenny, *J. Mater. Chem.*, 2010, **20**, 995.
47 J. Geng and H.-T. Jung, *J. Phys. Chem. C*, 2010, **114**, 8227.
48 P. Viet Hung, C. Tran Viet, S. H. Hur, E. Oh, E. J. Kim, E. W. Shin and J. S. Chung, *J. Mater. Chem.*, 2011, **21**, 3371.
49 X.-D. Zhuang, Y. Chen, G. Liu, P.-P. Li, C.-X. Zhu, E.-T. Kang, K.-G. Neoh, B. Zhang, J.-H. Zhu and Y.-X. Li, *Adv. Mater.*, 2010, **22**, 1731.
50 X.-L. Zhang, X. Zhao, Z.-B. Liu, Y.-S. Liu, Y.-S. Chen and J.-G. Tian, *Opt. Express*, 2009, **17**, 23959.
51 Y. Xu, Z. Liu, X. Zhang, Y. Wang, J. Tian, Y. Huang, Y. Ma, X. Zhang and Y. Chen, *Adv. Mater.*, 2009, **21**, 1275.
52 E. Kymakis and G. Amaratunga, *Appl. Phys. Lett.*, 2002, **80**, 112.
53 E. Kymakis, I. Alexandrou and G. Amaratunga, *J. Appl. Phys.*, 2003, **93**, 1764.
54 T. Schuettfort, H. Snaith, A. Nish and R. Nicholas, *Nanotechnology*, 2010, **21**, 025201.
55 M. Bernardi, M. Giulianini and J. C. Grossman, *ACS Nano*, 2010, **4**, 6599.
56 A. F. Nogueira, B. S. Lomba, M. A. Soto-Oviedo, C. R. D. Correia, P. Corio, C. A. Furtado and I. A. Hümmelgen, *J. Phys. Chem. C*, 2007, **111**, 18431.
57 M. Li, P. Xu, J. Yang, H. Ying, K. Haubner, L. Dunsch and S. Yang, *J. Phys. Chem. C*, 2011, **115**, 4584.
58 C.-K. Chang, J.-Y. Hwang, W.-J. Lai, C.-W. Chen, C.-I. Huang, K.-H. Chen and L.-C. Chen, *J. Phys. Chem. C*, 2010, **114**, 10932.
59 M.-H. Ham, G. L. C. Paulus, C. Y. Lee, C. Song, K. Kalantar-zadeh, W. Choi, J.-H. Han and M. S. Strano, *ACS Nano*, 2010, **4**, 6251.
60 F. Previti, S. Patane and M. Allegrini, *Appl. Surf. Sci.*, 2009, **255**, 9877.
61 J. Geng and T. Zeng, *J. Am. Chem. Soc.*, 2006, **128**, 16827.
62 Y. Kanai and J. C. Grossman, *Nano Lett.*, 2008, **8**, 908.
63 N. M. Dissanayake and Z. Zhong, *Nano Lett.*, 2011, **11**, 286.
64 A. J. Miller, R. A. Hatton and S. R. P. Silva, *Appl. Phys. Lett.*, 2006, **89**, 123115.
65 J. Arranz-Andres and W. J. Blau, *Carbon*, 2008, **46**, 2067.
66 I. Khatri, S. Adhikari, H. R. Aryal, T. Soga, T. Jimbo and M. Umeno, *Appl. Phys. Lett.*, 2009, **94**, 093509.
67 H. Ago, M. S. P. Shaffer, D. S. Ginger, A. H. Windle and R. H. Friend, *Phys. Rev. B: Condens. Matter*, 2000, **61**, 2286.
68 K. Kim, J. W. Shin, Y. B. Lee, M. Y. Cho, S. H. Lee, D. H. Park, D. K. Jang, C. J. Lee and J. Joo, *ACS Nano*, 2010, **4**, 4197.
69 Y. D. Park, J. A. Lim, Y. Jang, M. Hwang, H. S. Lee, D. H. Lee, H.-J. Lee, J.-B. Baek and K. Cho, *Org. Electron.*, 2008, **9**, 317.
70 Y. J. Song, J. U. Lee and W. H. Jo, *Carbon*, 2010, **48**, 389.
71 A. R. Inigo, S. J. Henley and S. R. P. Silva, *Nanotechnology*, 2011, **22**, 265711.
72 J. N. Coleman, S. Curran, A. B. Dalton, A. P. Davey, B. McCarthy, W. Blau and R. C. Barklie, *Phys. Rev. B: Condens. Matter*, 1998, **58**, R7492.
73 I. Alexandrou, E. Lioudakis, D. Delaportas, C. Z. Zhao and A. Othonos, *Nanoscale Res. Lett.*, 2009, **4**, 635.
74 Z. Xu, Y. Wu, B. Hu, I. N. Ivanov and D. B. Geohegan, *Appl. Phys. Lett.*, 2005, **87**, 263118.
75 E. Kymakis, P. Servati, P. Tzanetakis, E. Koudoumas, N. Kornilios, I. Rompogiannakis, Y. Franghiadakis and G. A. J. Amaratunga, *Nanotechnology*, 2007, **18**, 435702.
76 V. Saini, Z. Li, S. Bourdo, E. Dervishi, Y. Xu, X. Ma, V. P. Kunets, G. J. Salamo, T. Viswanathan, A. R. Biris, D. Saini and A. S. Biris, *J. Phys. Chem. C*, 2009, **113**, 8023.
77 S. Bhattacharyya, E. Kymakis and G. A. J. Amaratunga, *Chem. Mater.*, 2004, **16**, 4819.

78 C. Li, Y. Chen, Y. Wang, Z. Iqbal, M. Chhowalla and S. Mitra, *J. Mater. Chem.*, 2007, **17**, 2406.
79 N. Tezuka, T. Umeyama, Y. Matano, T. Shishido, K. Yoshida, T. Ogawa, S. Isoda, K. Stranius, V. Chukharev, N. V. Tkachenko, H. Lemmetyinen and H. Imahori, *Energy Environ. Sci.*, 2011, **4**, 741.
80 B. J. Landi, R. P. Raffaelle, S. L. Castro and S. G. Bailey, *Progr. Photovolt.: Res. Appl.*, 2005, **13**, 165.
81 B. Landi, S. Castro, H. Ruf, C. Evans, S. Bailey and R. Raffaelle, *Sol. Energy Mater. Sol. Cells*, 2005, **87**, 733.
82 G. Conturbia, R. d. C. G. Vinhas, R. Landers, G. M. S. Valente, V. Baranauskas and A. F. Nogueira, *J. Nanosci. Nanotechnol.*, 2009, **9**, 5850.
83 N. Cho, K. Roy Choudhury, R. B. Thapa, Y. Sahoo, T. Ohulchanskyy, A. N. Cartwright, K. S. Lee and P. N. Prasad, *Adv. Mater.*, 2007, **19**, 232.
84 L. M. Chen, Z. Xu, Z. Hong and Y. Yang, *J. Mater. Chem.*, 2010, **20**, 2575.
85 R. Steim, F. R. Kogler and C. J. Brabec, *J. Mater. Chem.*, 2010, **20**, 2499.
86 S. Berson, R. de Bettignies, S. Bailly, S. Guillerez and B. Jousselme, *Adv. Funct. Mater.*, 2007, **17**, 3363.
87 E. Kymakis, N. Kornilios and E. Koudoumas, *J. Phys. D: Appl. Phys.*, 2008, **41**, 165110.
88 J. Geng, B.-S. Kong, S. B. Yang, S. C. Youn, S. Park, T. Joo and H.-T. Jung, *Adv. Funct. Mater.*, 2008, **18**, 2659.
89 V. Sadhu, N. A. Nismy, A. A. D. T. Adikaari, S. J. Henley, M. Shkunov and S. R. P. Silva, *Nanotechnology*, 2011, **22**, 265607.
90 L. Liu, W. E. Stanchina and G. Li, *Appl. Phys. Lett.*, 2009, **94**, 233309.
91 M.-C. Wu, Y.-Y. Lin, S. Chen, H.-C. Liao, Y.-J. Wu, C.-W. Chen, Y.-F. Chen and W.-F. Su, *Chem. Phys. Lett.*, 2009, **468**, 64.
92 L. Liu and G. Li, *Appl. Phys. Lett.*, 2010, **96**, 083302.
93 A. T. Mallajosyula, S. S. K. Iyer and B. Mazhari, *J. Appl. Phys.*, 2011, **109**, 124908.
94 B. K. Kuila, K. Park and L. Dai, *Macromolecules*, 2010, **43**, 6699.
95 A. P. Le, T.-M. Huang, P.-T. Chen and A. C.-M. Yang, *J. Polym. Sci., Part B: Polym. Phys.*, 2011, **49**, 581.
96 J. M. Lee, J. S. Park, S. H. Lee, H. Kim, S. Yoo and S. O. Kim, *Adv. Mater.*, 2011, **23**, 629.
97 H. Derbal-Habak, C. Bergeret, J. Cousseau and J. M. Nunzi, *Sol. Energy Mater. Sol. Cells*, 2011, **95**, S53.
98 R. K. Singh, J. Kumar, A. Kumar, V. Kumar, R. Kant and R. Singh, *Sol. Energy Mater. Sol. Cells*, 2010, **94**, 2386.
99 J. G. Wang, Y. S. Wang, D. W. He, H. P. Wu, H. T. Wang, P. Zhou, Y. N. Zhang and M. Fu, *Adv. Mater. Res.*, 2012, **396–398**, 2471.
100 J. Wang, Y. Wang, D. He, Z. Liu, H. Wu, H. Wang, P. Zhou and M. Fu, *Sol. Energy Mater. Sol. Cells*, 2012, **96**, 58.
101 Y. Gao, H.-L. Yip, K.-S. Chen, K. M. O'Malley, O. Acton, Y. Sun, G. Ting, H. Chen and A. K. Y. Jen, *Adv. Mater.*, 2011, **23**, 1903.
102 H. Chang, G. Wang, A. Yang, X. Tao, X. Liu, Y. Shen and Z. Zheng, *Adv. Funct. Mater.*, 2010, **20**, 2893.
103 J. Kim, V. C. Tung and J. Huang, *Adv. Energy Mater.*, 2011, **1**, 1052.
104 V. C. Tung, J. Kim, L. J. Cote and J. Huang, *J. Am. Chem. Soc.*, 2011, **133**, 9262.
105 Z. Liu, Q. Liu, Y. Huang, Y. Ma, S. Yin, X. Zhang, W. Sun and Y. Chen, *Adv. Mater.*, 2008, **20**, 3924.
106 W. S. HummersJr and R. E. Offeman, *J. Am. Chem. Soc.*, 1958, **80**, 1339.
107 H. Chang, Y. Liu, H. Zhang and J. Li, *J. Electroanal. Chem.*, 2011, **656**, 269.
108 Z. Liu, D. He, Y. Wang, H. Wu, J. Wang and H. Wang, *Sol. Energy Mater. Sol. Cells*, 2010, **94**, 2148.
109 Z. Liu, D. He, Y. Wang, H. Wu and J. Wang, *Synth. Met.*, 2010, **160**, 1036.
110 S.-S. Li, K.-H. Tu, C.-C. Lin, C.-W. Chen and M. Chhowalla, *ACS Nano*, 2010, **4**, 3169.
111 D. Yu, Y. Yang, M. Durstock, J.-B. Baek and L. Dai, *ACS Nano*, 2010, **4**, 5633.
112 D. Yu, K. Park, M. Durstock and L. Dai, *J. Phys. Chem. Lett.*, 2011, **2**, 1113.
113 C. M. Hill, Y. Zhu and S. Pan, *ACS Nano*, 2011, **5**, 942.
114 Y. Wang, D. Kurunthu, G. W. Scott and C. J. Bardeen, *J. Phys. Chem. C*, 2010, **114**, 4153.
115 A. Liscio, G. P. Veronese, E. Treossi, F. Suriano, F. Rossella, V. Bellani, R. Rizzoli, P. Samori and V. Palermo, *J. Mater. Chem.*, 2011, **21**, 2924.
116 J. E. Klare, I. P. Murray, J. Goldberger and S. I. Stupp, *Chem. Commun.*, 2009, 3705.
117 L. Picard, F. Lincker, Y. Kervella, M. Zagorska, R. DeBettignies, A. Peigney, E. Flahaut, G. Louarn, S. Lefrant and R. Demadrille, *J. Phys. Chem. C*, 2009, **113**, 17347.
118 T. Hasobe, S. Fukuzumi and P. V. Kamat, *J. Phys. Chem. B*, 2006, **110**, 25477.
119 S. Campidelli, B. Ballesteros, A. Filoramo, D. D. Di az, G. de la Torre, T. Torres, G. M. A. Rahman, C. Ehli, D. Kiessling and F. Werner, *J. Am. Chem. Soc.*, 2008, **130**, 11503.
120 S. Campidelli, C. Sooambar, E. L. Diz, C. Ehli, D. M. Guldi and M. Prato, *J. Am. Chem. Soc.*, 2006, **128**, 12544.
121 A. Chunder, T. Pal, S. I. Khondaker and L. Zhai, *J. Phys. Chem. C*, 2010, **114**, 15129.
122 N. Karousis, A. S. D. Sandanayaka, T. Hasobe, S. P. Economopoulos, E. Sarantopoulou and N. Tagmatarchis, *J. Mater. Chem.*, 2011, **21**, 109.
123 A. Wojcik and P. V. Kamat, *ACS Nano*, 2010, **4**, 6697.
124 X. Zhang, Y. Feng, S. Tang and W. Feng, *Carbon*, 2010, **48**, 211.
125 S. B. Bon, L. Valentini, R. M. Moustafa, F. M. Jradi, B. R. Kaafarani, R. Verdejo, M. A. Lopez-Manchado and J. M. Kenny, *J. Phys. Chem. C*, 2010, **114**, 11252.
126 B. M. Kayes, H. A. Atwater and N. S. Lewis, *J. Appl. Phys.*, 2005, **97**, 114302.
127 S. M. Wong, H. Y. Yu, J. S. Li, Y. L. Li, N. Singh, P. G. Q. Lo and D. L. Kwong, *IEEE Electron Device Lett.*, 2011, **32**, 176.
128 K. Q. Peng, Z. P. Huang and J. Zhu, *Adv. Mater.*, 2004, **16**, 73.
129 K. Q. Peng, Y. Wu, H. Fang, X. Y. Zhong, Y. Xu and J. Zhu, *Angew. Chem., Int. Ed.*, 2005, **44**, 2737.
130 E. Garnett and P. Yang, *Nano Lett.*, 2010, **10**, 1082.
131 O. Gunawan, K. Wang, B. Fallahazad, Y. Zhang, E. Tutuc and S. Guha, *Prog. Photovoltaics*, 2011, **19**, 307.
132 J. Kim, A. J. Hong, J.-W. Nah, B. Shin, F. M. Ross and D. K. Sadana, *ACS Nano*, 2011, **6**, 265.
133 L. Sainiemi, V. Jokinen, A. Shah, M. Shpak, S. Aura, P. Suvanto and S. Franssila, *Adv. Mater.*, 2011, **23**, 122.
134 L. Tsakalakos, J. Balch, J. Fronheiser, B. A. Korevaar, O. Sulima and J. Rand, *Appl. Phys. Lett.*, 2007, **91**, 233117.
135 G. Yuan, H. Zhao, X. Liu, Z. S. Hasanali, Y. Zou, A. Levine and D. Wang, *Angew. Chem., Int. Ed.*, 2009, **48**, 9680.
136 S. W. Boettcher, J. M. Spurgeon, M. C. Putnam, E. L. Warren, D. B. Turner-Evans, M. D. Kelzenberg, J. R. Maiolo, H. A. Atwater and N. S. Lewis, *Science*, 2010, **327**, 185.
137 M. C. Putnam, S. W. Boettcher, M. D. Kelzenberg, D. B. Turner-Evans, J. M. Spurgeon, E. L. Warren, R. M. Briggs, N. S. Lewis and H. A. Atwater, *Energy Environ. Sci.*, 2010, **3**, 1037.
138 S. W. Boettcher, E. L. Warren, M. C. Putnam, E. A. Santori, D. Turner-Evans, M. D. Kelzenberg, M. G. Walter, J. R. McKone, B. S. Brunschwig, H. A. Atwater and N. S. Lewis, *J. Am. Chem. Soc.*, 2011, **133**, 1216.
139 Y. Dan, K. Seo, K. Takei, J. H. Meza, A. Javey and K. B. Crozier, *Nano Lett.*, 2011, **11**, 2527.
140 M. D. Kelzenberg, D. B. Turner-Evans, B. M. Kayes, M. A. Filler, M. C. Putnam, N. S. Lewis and H. A. Atwater, *Nano Lett.*, 2008, **8**, 710.
141 K. Q. Peng, Y. Xu, Y. Wu, Y. J. Yan, S. T. Lee and J. Zhu, *Small*, 2005, **1**, 1062.
142 K. Peng, X. Wang and S.-T. Lee, *Appl. Phys. Lett.*, 2008, **92**, 163103.
143 H. Fang, X. Li, S. Song, Y. Xu and J. Zhu, *Nanotechnology*, 2008, **19**, 255703.
144 E. A. Dalchiele, F. Martin, D. Leinen, R. E. Marotti and J. Ramon Ramos-Barrado, *J. Electrochem. Soc.*, 2009, **156**, K77.
145 V. Sivakov, G. Andrae, A. Gawlik, A. Berger, J. Plentz, F. Falk and S. H. Christiansen, *Nano Lett.*, 2009, **9**, 1549.
146 Z. Jia, X. Yueqing, W. Qi and C. Yi *Photovoltaic Specialists Conference (PVSC)*, 35th IEEE, 2010; p 000453.
147 M. J. Naughton, K. Kempa, Z. F. Ren, Y. Gao, J. Rybczynski, N. Argenti, W. Gao, Y. Wang, Y. Peng, J. R. Naughton, G. McMahon, T. Paudel, Y. C. Lan, M. J. Burns, A. Shepard, M. Clary, C. Ballif, F. J. Haug, T. Soederstroem, O. Cubero and C. Eminian, *Phys. Status Solidi RRL*, 2010, **4**, 181.
148 S. M. Wong, H. Y. Yu, Y. Li, J. Li, X. W. Sun, N. Singh, P. G. Q. Lo and D.-L. Kwong, *IEEE Trans. Electron Devices*, 2011, **58**, 3224.
149 J.-Y. Jung, Z. Guo, S.-W. Jee, H.-D. Um, K.-T. Park, M. S. Hyun, J. M. Yang and J.-H. Lee, *Nanotechnology*, 2010, **21**, 445303.

150 G. Fan, H. Zhu, K. Wang, J. Wei, X. Li, Q. Shu, N. Guo and D. Wu, *ACS Appl. Mater. Interfaces*, 2011, **3**, 721.
151 Q. Shu, J. Wei, K. Wang, H. Zhu, Z. Li, Y. Jia, X. Gui, N. Guo, X. Li, C. Ma and D. Wu, *Nano Lett.*, 2009, **9**, 4338.
152 H. P. Yoon, Y. A. Yuwen, C. E. Kendrick, G. D. Barber, N. J. Podraza, J. M. Redwing, T. E. Mallouk, C. R. Wronski and T. S. Mayer, *Appl. Phys. Lett.*, 2010, **96**, 213503.
153 A. Boukai, P. Haney, A. Katzenmeyer, G. M. Gallatin, A. A. Talin and P. Yang, *Chem. Phys. Lett.*, 2011, **501**, 153.
154 J. M. G. Laranjeira, H. J. Khoury, W. M. de Azevedo, E. F. da Silva and E. A. de Vasconcelos, *Appl. Surf. Sci.*, 2002, **190**, 390.
155 Q. Wang, S. E. Shaheen, E. L. Williams and G. E. Jabbour, *Appl. Phys. Lett.*, 2003, **83**, 3404.
156 W. Wang and E. A. Schiff, *Appl. Phys. Lett.*, 2007, **91**, 133504.
157 J. C. Nolasco, R. Cabre, J. Ferre-Borrull, L. F. Marsal, M. Estrada and J. Pallares, *J. Appl. Phys.*, 2010, **107**, 044505.
158 C.-H. Lin, S. Chattopadhyay, C.-W. Hsu, M.-H. Wu, W.-C. Chen, C.-T. Wu, S.-C. Tseng, J.-S. Hwang, J.-H. Lee, C.-W. Chen, C.-H. Chen, L.-C. Chen and K.-H. Chen, *Adv. Mater.*, 2009, **21**, 759.
159 C.-H. Chao, C.-H. Chan, F.-C. Wu, J.-J. Huang, S. Y. Lien, K.-W. Weng and H.-L. Cheng, *Sol. Energy Mater. Sol. Cells*, 2011, **95**, 2407.
160 G. Zou, H. Luo, F. Ronning, B. Sun, T. M. McCleskey, A. K. Burrell, E. Bauer and Q. X. Jia, *Angew. Chem., Int. Ed.*, 2010, **49**, 1782.
161 M. J. Sailor, E. J. Ginsburg, C. B. Gorman, A. Kumar, R. H. Grubbs and N. S. Lewis, *Science*, 1990, **249**, 1146.
162 Y. Jia, J. Wei, K. Wang, A. Cao, Q. Shu, X. Gui, Y. Zhu, D. Zhuang, G. Zhang, B. Ma, L. Wang, W. Liu, Z. Wang, J. Luo and D. Wu, *Adv. Mater.*, 2008, **20**, 4594.
163 S. Avasthi, S. Lee, Y.-L. Loo and J. C. Sturm, *Adv. Mater.*, 2011, **23**, 5762.
164 A. A. D. T. Adikaari, D. M. N. M. Dissanayake, R. A. Hatton and S. R. P. Silva, *Appl. Phys. Lett.*, 2007, **90**, 203514.
165 L. Zhao, Q. Chen, C. Li and G. Shi, *Sol. Energy Mater. Sol. Cells*, 2007, **91**, 1811.
166 C. H. Peters, A. R. Guichard, A. C. Hryciw, M. L. Brongersma and M. D. McGehee, *J. Appl. Phys.*, 2009, **105**, 124509.
167 Z. Pei, S. Thiyagu, M.-S. Jhong, W.-S. Hsieh, S.-J. Cheng, M.-W. Ho, Y.-H. Chen, J.-C. Liu and C.-M. Yeh, *Sol. Energy Mater. Sol. Cells*, 2011, **95**, 2431.
168 J. M. Spurgeon, S. W. Boettcher, M. D. Kelzenberg, B. S. Brunschwig, H. A. Atwater and N. S. Lewis, *Adv. Mater.*, 2010, **22**, 3277.
169 J. M. Spurgeon, M. G. Walter, J. Zhou, P. A. Kohl and N. S. Lewis, *Energy Environ. Sci.*, 2011, **4**, 1772.
170 M. D. Kelzenberg, S. W. Boettcher, J. A. Petykiewicz, D. B. Turner-Evans, M. C. Putnam, E. L. Warren, J. M. Spurgeon, R. M. Briggs, N. S. Lewis and H. A. Atwater, *Nat. Mater.*, 2010, **9**, 239.
171 J.-S. Huang, C.-Y. Hsiao, S.-J. Syu, J.-J. Chao and C.-F. Lin, *Sol. Energy Mater. Sol. Cells*, 2009, **93**, 621.
172 J.-M. Yun, J.-S. Yeo, J. Kim, H.-G. Jeong, D.-Y. Kim, Y.-J. Noh, S.-S. Kim, B.-C. Ku and S.-I. Na, *Adv. Mater.*, 2011, **23**, 4923.
173 Y. Gao, H.-L. Yip, S. K. Hau, K. M. O'Malley, N. C. Cho, H. Chen and A. K. Y. Jen, *Appl. Phys. Lett.*, 2010, **97**, 203306.
174 C. E. Small, S. Chen, J. Subbiah, C. M. Amb, S.-W. Tsang, T.-H. Lai, J. R. Reynolds and F. So, *Nat. Photonics*, 2011, DOI: 10.1038/nphoton.2011.317.
175 C. Y. Kuo and C. Gau, *Appl. Phys. Lett.*, 2009, **95**, 053302.
176 G. Kalita, S. Adhikari, H. R. Aryal, R. Afre, T. Soga, M. Sharon, W. Koichi and M. Umeno, *J. Phys. D: Appl. Phys.*, 2009, **42**, 115104.
177 E. C. Garnett and P. Yang, *J. Am. Chem. Soc.*, 2008, **130**, 9224.
178 D. R. Kim, C. H. Lee, P. M. Rao, I. S. Cho and X. Zheng, *Nano Lett.*, 2011, **11**, 2704.
179 M. Y. Bashouti, R. T. Tung and H. Haick, *Small*, 2009, **5**, 2761.
180 F. Zhang, B. Sun, T. Song, X. Zhu and S. Lee, *Chem. Mater.*, 2011, **23**, 2084.
181 V. Gowrishankar, S. R. Scully, A. T. Chan, M. D. McGehee, Q. Wang and H. M. Branz, *J. Appl. Phys.*, 2008, **103**, 064511.
182 K.-Q. Peng, X. Wang, X.-L. Wu and S.-T. Lee, *Nano Lett.*, 2009, **9**, 3704.
183 S.-C. Shiu, J.-J. Chao, S.-C. Hung, C.-L. Yeh and C.-F. Lin, *Chem. Mater.*, 2010, **22**, 3108.
184 L. Dai-Hong, S. Shu-Chia, H. Jing-Shun and L. Ching-Fuh *Photovoltaic Specialists Conference (PVSC)*, 35th IEEE, 2010; p 000949.
185 E. C. Garnett, C. Peters, M. Brongersma, C. Yi and M. McGehee *Photovoltaic Specialists Conference (PVSC)*, 35th IEEE, 2010; p 000934.
186 B. Ozdemir, M. Kulakci, R. Turan and H. E. Unalan, *Appl. Phys. Lett.*, 2011, **99**, 113510.
187 W. Lu, C. Wang, W. Yue and L. Chen, *Nanoscale*, 2011, **3**, 3631.
188 H. Lining, Rusli, J. Changyun, W. Hao and D. Lai, *IEEE Electron Device Lett.*, 2011, **32**, 1406.
189 M. J. Price, J. M. Foley, R. A. May and S. Maldonado, *Appl. Phys. Lett.*, 2010, **97**, 083503.
190 I. A. Levitsky, W. B. Euler, N. Tokranova, B. Xu and J. Castracane, *Appl. Phys. Lett.*, 2004, **85**, 6245.
191 G. A. Il'chuk, N. V. Klimova, O. I. Kon'kov, S. E. Nikitin, Y. A. Nikolaev, L. I. Rudaya, V. Y. Rud, Y. V. Rud, E. I. Terukov, V. V. Shamanin and T. A. Yurre, *Semiconductors*, 2004, **38**, 1018.
192 M. M. El-Nahass, H. M. Zeyada, M. S. Aziz and M. M. Makhlouf, *Thin Solid Films*, 2005, **492**, 290.
193 C. B. Winkelmann, I. Ionica, X. Chevalier, G. Royal, C. Bucher and V. Bouchiat, *Nano Lett.*, 2007, **7**, 1454.
194 L. Wen, X. Liu, N. Yang, J. Zhai, C. Huang, Y. Li and L. Jiang, *Appl. Phys. Lett.*, 2010, **97**, 253111.
195 R. Prabakaran, E. Fortunato, R. Martins and I. Ferreira, *J. Non-Cryst. Solids*, 2008, **354**, 2892.
196 L.-C. Chen and B.-H. Liu, *Electrochem. Solid-State Lett.*, 2010, **13**, H108.
197 L. He, C. Jiang, D. Lai and H. Wang, *Appl. Phys. Lett.*, 2011, **99**, 021104.
198 X. Shen, B. Sun, D. Liu and S.-T. Lee, *J. Am. Chem. Soc.*, 2011, **133**, 19408.
199 Z. Kang, Y. Liu and S.-T. Lee, *Nanoscale*, 2011, **3**, 777.
200 V. Svrcek, *Pure Appl. Chem.*, 2010, **82**, 2121.
201 V. Svrcek, H. Fujiwara and M. Kondo, *Appl. Phys. Lett.*, 2008, **92**, 143301.
202 Z. C. Holman, C.-Y. Liu and U. R. Kortshagen, *Nano Lett.*, 2010, **10**, 2661.
203 X. Pi, Q. Li, D. Li and D. Yang, *Sol. Energy Mater. Sol. Cells*, 2011, **95**, 2941.
204 S. Park, E. Cho, D. Song, G. Conibeer and M. A. Green, *Sol. Energy Mater. Sol. Cells*, 2009, **93**, 684.
205 M. C. Beard, K. P. Knutsen, P. Yu, J. M. Luther, Q. Song, W. K. Metzger, R. J. Ellingson and A. J. Nozik, *Nano Lett.*, 2007, **7**, 2506.
206 A. J. Nozik, *Chem. Phys. Lett.*, 2008, **457**, 3.
207 V. Švrček, S. Cook, S. Kazaoui and M. Kondo, *J. Phys. Chem. Lett.*, 2011, **2**, 1646.
208 C.-Y. Liu and U. R. Kortshagen, *Nanoscale Res. Lett.*, 2010, **5**, 1253.
209 V. Švrček, D. Mariotti, Y. Shibata and M. Kondo, *J. Phys. D: Appl. Phys.*, 2010, **43**, 415402.
210 R. Dietmueller, A. R. Stegner, R. Lechner, S. Niesar, R. N. Pereira, M. S. Brandt, A. Ebbers, M. Trocha, H. Wiggers and M. Stutzmann, *Appl. Phys. Lett.*, 2009, **94**, 113301.
211 C.-Y. Liu, Z. C. Holman and U. R. Kortshagen, *Adv. Funct. Mater.*, 2010, **20**, 2157.
212 S. Niesar, R. Dietmueller, H. Nesswetter, H. Wiggers and M. Stutzmann, *Phys. Status Solidi A*, 2009, **206**, 2775.
213 L. Chen, X. Pan, D. Zheng, Y. Gao, X. Jiang, M. Xu and H. Chen, *Nanotechnology*, 2010, **21**, 345201.
214 B. Eisenhawer, S. Sensfuss, V. Sivakov, M. Pietsch, G. Andrae and F. Falk, *Nanotechnology*, 2011, **22**, 315401.

